EFFECT OF PARTICLE BREAKAGE ON BALLAST PERMANENT DEFORMATION – A STUDY USING THE DISCRETE ELEMENT METHOD

by

Beema Dahal

A thesis

submitted in partial fulfilment

of the requirements for the degree of

Master of Science in Civil Engineering

Boise State University

December 2018

BOISE STATE UNIVERSITY GRADUATE COLLEGE

DEFENSE COMMITTEE AND FINAL READING APPROVALS

of the thesis submitted by

Beema Dahal

Thesis Title: Effect of Particle Breakage on Ballast Permanent Deformation – A Study Using the Discrete Element Method

Date of Final Oral Examination: 1 November 2018

The following individuals read and discussed the thesis submitted by student Beema Dahal, and they evaluated her presentation and response to questions during the final oral examination. They found that the student passed the final oral examination.

Debakanta Mishra, Ph.D.	Chair, Supervisory Committee
Bhaskar Chittoori, Ph.D.	Member, Supervisory Committee
David Potyondy, Ph.D.	Member, Supervisory Committee

The final reading approval of the thesis was granted by Debakanta Mishra, Ph.D., Chair of the Supervisory Committee. The thesis was approved by the Graduate College.

DEDICATION

Dedicated to my late brother Sanjay Dahal

We miss you

ACKNOWLEDGMENTS

I would like to express my sincere gratitude to my advisor, Dr. Debakanta Mishra, who always encouraged me to do innovative research. His welcoming nature, kind appreciation, timely feedback and unparalleled guidance motivated and made me the confident researcher I had always aspired to be.

I also wish to express my gratitude to Dr. Bhaskar Chittoori and Dr. David Potyondy for serving on my Supervisory Committee. The contributions of SM Naziur Mahmud of Boise State University for helping me learn the software and his guidance are highly acknowledged. I also want to thank the Mishra Research Group and all the graduate student researchers in the Civil Engineering Department for their support and for making my stay at Boise State memorable.

Finally, I would like to thank my family members for their continued support in every step of my life.

ABSTRACT

The ballast layer comprises relatively large (often as large as 63 mm) angular particles that mainly function to dissipate train-induced stresses from crossties to the underlying subgrade soils and to provide rapid drainage for surface water. Moreover, the ballast layer is also critical towards ensuring a smooth riding track profile, dampening dynamic loads, as well as providing lateral, longitudinal and vertical resistance against excessive track deformations. Under train loading and during track maintenance processes like tamping, individual ballast particles can undergo significant breakage leading to fouling of the ballast layer. The fouling mechanism leads to gradual deterioration in ballast shear strength as well as drainage properties. Inadequate drainage of surface water can lead to further reduction in the ballast layer's ability to resist excessive track deformations, ultimately leading to geometric defects such as severely ill-conditioned geometry parameters like profile, alignment, gauge, cant and twist. About 76% of the fouling in a ballast layer can be attributed to ballast degradation and breakdown under repeated train loading. In extreme cases, ballast breakage may potentially lead to derailment as a major portion of track vertical settlement or permanent deformation occurs within the ballast layer. Several researchers in the past have studied the phenomenon of ballast breakage in a laboratory setting. However, due to complexities associated with these large-scale laboratory tests, detailed parametric studies are often not feasible. In such cases, numerical modeling tools such as the Discrete Element Method (DEM) become particularly useful. This master's thesis presents findings from a research study aimed at understanding the

significance of ballast breakage considerations in the associated vertical permanent deformation of the ballast layer under repeated loading. A commercially available Discrete Element Package (PFC3D®) was used to simulate the response of the ballast layer under loading. Various factors that affect ballast breakage and eventual permanent deformation accumulation within the ballast layer were studied, and analyzed. First, the ballast particles were modeled using simple ellipsoid shapes. Parametric studies were conducted to quantify the effects of different parameters such as cyclic load amplitude, loading frequency, number of loading cycles, particle strength, and particle size distribution. As a subsequent enhancement to the research approach, laboratory tests were conducted to quantify the crushing strengths of individual ballast particles. A DEM model was prepared to simulate the Single Particle Crushing Test (SPCT), and calibrated against the laboratory test results. The calibrated parameters were then used to study the response of polyhedral ballast particles (simulated as clumps in PFC3D®) under repeated loading. Comparisons of permanent deformation and ballast breakage were made for polyhedral ballast particles and ellipsoid ballast particles. From the results, it was observed that there was a significant deviation in permanent deformation (polyhedral ballast layer underwent 80% more permanent deformation than the ellipsoid ballast layer). When the relative shift in particle distribution curves (the area between the particle size distribution curves before and after loading), were compared for the ellipsoid and polyhedral ballast layers it was seen that polyhedral ballasts underwent about 53% more breakage compared to ellipsoid ballasts. This showed the importance of polyhedral shape simulation to accurately study ballast layer response under loading. As a potential approach to reduce ballast breakage and permanent deformation, the model was subsequently modified to incorporate geogrid

reinforcement. Two different geogrid types, with square and triangular aperture, were modeled, and the response of geogrid-reinforced ballast layers were compared against unreinforced configurations. From the results, it was seen that the unreinforced ballast layer showed the highest permanent axial strain (approximately 15%), and the same for all the geogrid-embedded ballast layers were found to be approximately 10%. This showed that geogrid reinforcement reduces permanent deformation accumulation within the ballast layer. However, no significant effect of geogrid reinforcement was observed when the extent of ballast breakage was compared. Detailed understanding of different factors governing ballast breakage and permanent deformation accumulation can help facilitate the design and construction of better performing railroad tracks.

TABLE OF CONTENTS

LIST OF TABLES

LIST OF FIGURES

CHAPTER 1: INTRODUCTION AND BACKGROUND

Statement of Problem

In the early 20th century, also called the "Golden Era" for the railroads, there were more than 190,000 miles of railroads in service in the United States (American-rails, 2016). This boom, however, took a U-turn as trains lost their "shine" during the post-World War II period, whereby many railroad lines were abandoned (American-rails, 2016). This was due to inclination of the population towards other modes of transportation like airplanes and automobiles, as they offered better operational speeds and cost-effectiveness. However, recently, railroads have made a strong comeback as freight as well as passenger traffic have increased significantly since 2010 (Ostria, 2004; Neff and Dickens, 2013), and are expected to increase even more in the future. This increase can be attributed to the fact that railroads are fuel efficient, environment-friendly, offer greater safety, and present a quicker mode for intercity transportation (Indraratna et al., 1998). The demand for faster and higher load capacity trains has also been increasing owing to the ever-increasing traffic congestions and fuel costs (Mahmud, 2017). Construction and maintenance of structurally and functionally efficient railroads demand significant annual investments which necessitate an in-depth understanding of track mechanics, and track response under loading.

In a conventional track structure, the ballast layer represents an integral component. It comprises coarse-grained (often as large as 63 mm in size) aggregate particles, and constitutes the top layer of the track substructure, placed in the crib areas between sleepers,

and in shoulders beyond the tie ends. The ballast layer serves various functions such as distributing train-induced loads from the sleepers to the underlying subgrade layer (ensuring the stress levels on top of the subgrade do not exceed recommended values), providing lateral resistance against track deformation, facilitating rapid drainage of surface water, and also providing a damping medium against dynamic train loads. A well-performing ballast layer should ideally possess optimum drainage and shear strength properties. However, under train-induced repeated loading, ballast particles can undergo significant amount of breakage, leading to track geometry defects. Moreover, track resurfacing activities such as tamping have also been reported to cause ballast breakage (Wright, 1983; Saussine et al., 2008). Gradual breakage of ballast particles leads to a change in the ballast gradation. This phenomenon of gradual contamination of the ballast layer by fines (originating either from breakage of ballast particles, or from contamination with external fine particles such as subgrade soils, coal dust, etc.) is referred to as “fouling”. Selig and Waters (1994) reported that a major portion (approximately 76%) of ballast layer fouling occurs due to breakdown of ballast particles. The strength and deformation response of ballast under loading is significantly influenced by particle breakage (Indraratna et al., 1998; Anderson and Key, 2000). Besides leading to reduced shear strength of the ballast layer, excessive particle breakage also results in poor drainage, pumping of underlying soft subgrade soils and unacceptable differential settlement of track, which eventually necessitate frequent track maintenance (Indraratna and Nimbalkar, 2011); maintenance costs related to restoring ballast layer condition have been found to be very high (Indraratna et al., 1998; Lobo-Guerrero and Vallejo, 2006). Excessive deterioration in the ballast layer condition often causes rapid deterioration of the track

geometry, requiring speed restrictions, and in extreme cases can cause derailment. Past research studies have also observed that the ballast layer accounts for a major portion of total track settlement (Selig and Waters, 1994; Mishra et al., 2014). Proper understanding of the effects of ballast breakage on the permanent deformation can potentially facilitate the optimization of track substructure design, ultimately leading to a reduction in recurrent track maintenance costs.

Background

Various researchers in the past have conducted laboratory and field experiments on ballast layers to understand the effects of particle breakage on ballast permanent deformation under loading (Indraratna et al., 1998; Aursudkij et al., 2009; Shenton, 1975). Field tests can capture actual ballast response, but owing to large particle-size (often as large as 63 mm) of railroad ballast, significantly large specimens have to be tested in the laboratory for realistic estimation of the ballast response without introducing undesirable boundary effects. Applying cyclic loading on laboratory and field ballast samples, and performing parametric studies to quantify the effects of different material, specimen, and test variables on behavior under loading is often not feasible in standard geotechnical engineering laboratories (Mahmud, 2017). These experiments also cannot provide a complete picture regarding the commencement and evolution of ballast breakage (Indraratna et al., 2010). In such situations, numerical modeling tools such as the Discrete Element Method (DEM) can become logical alternatives to facilitate in-depth understanding of material behavior as they can effectively model the discrete nature of the ballast particles. These numerical simulations simplify the nature, shape and interactions between ballast particles, but can effectively show how the degradation process initiates

and evolves under loading, and how it influences permanent deformation of ballast layers (Lobo-Guerrero and Vallejo, 2006). Several researchers (Lobo-Guerrero and Vallejo, 2006; Indraratna et al., 2010) have used DEM simulations to study the process of ballast breakage under loading. Conducting parametric studies using DEM is much more practical as specimen parameters can be accurately controlled, while isolating the factors being investigated.

Discrete Element Method as a Numerical Modeling Tool

The Discrete Element Method (also referred to as the Distinct Element Method) is a numerical method developed by Peter Cundall in 1971 (Cundall, 1971) to study the motion of individual discrete particles. DEM allows finite displacements and rotations of discrete bodies, including complete detachment, and recognizes new contacts automatically as the calculation progresses (Cundall and Hart, 1992). Externally applied forces and body forces create disturbance in the system of particles, which results in the propagation of movements of particles and by tracing the movements of these individual particles, contact forces and displacements of particle assemblies are found (Potyondy and Cundall, 2004; Potyondy, 2015). This dynamic process is said to reach a state of equilibrium when internal forces in the system balance (Potyondy and Cundall, 2004; Potyondy, 2015). The calculations performed in DEM alternate between the application of Newton's second law to the particles and a force–displacement law at the contacts (Cundall and Strack, 1979). Newton's second law is used to determine the translational and rotational motion of each particle arising from the contact forces, applied forces and body forces acting upon it; force–displacement law is used to update the contact forces arising from relative motion at each contact (Potyondy and Cundall, 2004; Potyondy, 2015). The dynamic behavior is

represented numerically by a time-stepping algorithm in which the velocities and accelerations are assumed to be constant within each time step. The solution scheme is identical to that used by the explicit finite-difference method for continuum analysis. The DEM is based on the idea that the time step chosen may be so small that during a single time step, disturbances cannot propagate from any particle farther than its immediate neighbors. Then, at all times, the forces acting on any particle are determined exclusively by its interaction with the particles with which it is in contact.

PFC3D® as a DEM tool

Particle Flow Code in 3 Dimensions (PFC3D®), a commercially available software, was used as the DEM tool in the current research effort. PFC3D provides a DEM framework that includes both a computational engine and a graphical user interface. PFC has been successfully used to solve problems ranging from fundamental research on soil and rock behavior at the laboratory scale to slope stability and rockfall hazard mitigation, hydraulic fracturing, rock-tool interactions, bulk flow, mixing, conveying and compaction of aggregates and powders, blast furnace modeling, etc. (Itasca, 2016). The PFC model provides a synthetic material that consists of an assembly of rigid grains interacting at contacts (Itasca 2016). The basic entities of PFC are balls, clumps, and walls which interact with one another via forces that arise at contacts. Contact models are assigned at the contacts between the bodies to define the contact behavior. The contact-model formulation provides a force-displacement law that relates the generalized internal force to the relative motion at the contact. The contact models provided with PFC are: Linear, Linear contact bond, Linear parallel bond, Hertz contact, Hysteretic contact, Smooth-joint contact, Flat-

Joint, Rolling resistance, Burger's model, and Hill contact model. More information about PFC can be found in PFC Documentation (Itasca, 2016).

Research Objectives and Tasks

Research Objective

The primary objective of this master's thesis research was to understand the significance of ballast breakage considerations on the permanent deformation behavior of railroad ballast layer under repeated loading. To start with, the following research questions were formulated:

1. Is it possible to get a better insight into the phenomenon of ballast breakage using the Discrete Element Method?
2. What factors govern the ballast breakage phenomenon?
3. Can the permanent deformation accumulation within ballast layers be significantly reduced by reducing the extent of ballast breakage?

To answer the above research questions, the following modeling steps were undertaken.

Modeling Step 1: Study the effects of various factors like number of load cycles (number of passes of train), applied vertical cyclic stress amplitude (maximum axle load that the ballast layer is subjected to), loading frequency (speed of train), particle size distribution and ballast particle strength to identify the relative importance of different factors that govern the permanent deformation behavior of railroad tracks under loading;

Modeling Step 2: Conduct laboratory crushing tests on real railroad ballast particles, calibrate a numerical model of the crushing test using the laboratory-obtained values;

Modeling Step 3: Study the effect of particle breakage on the permanent deformation behavior of ballast layers comprising complex-shaped ballast particles, simulated using agglomerates of spheres.

After completion of the above tasks, the following research hypothesis was formulated to study how permanent deformation in ballast layers can be reduced: *"Including a geogrid in the ballast layer can help reduce the extent of ballast breakage"*. The following modeling steps were carried out to check the validity of the research hypothesis.

Modeling Step 4: Study the effects of geogrid inclusion on ballast breakage and permanent deformation by modeling ballast layers reinforced with square- and triangular-aperture geogrids;

Modeling Step 5: Compare the effect of geogrid aperture shape on ballast breakage and permanent deformation accumulation.

The overall research hypothesis of this master's thesis was: "Reducing the extent of ballast breakage will reduce the associated permanent deformation accumulation under repeated loading".

Research Tasks and Manuscripts Prepared

The research tasks carried out under the scope of the current master's thesis were reported in the form of three technical manuscripts. The following table lists the individual tasks, and maps each of the tasks to the technical manuscripts prepared.

Table 1-1: Individual Research Tasks Mapped to Respective Manuscripts

Tasks	Name	Manuscripts
1	Ballast model generation using simple ellipsoid ballast shapes and application of cyclic load	Manuscript #1
2	Perform parametric study on the ballast model	
3	Post processing and plots generation	
4	Document and disseminate the results	
5	Simulate real ballast shapes for use in PFC3D	Manuscript #2
6	Laboratory Single Particle Crushing Test (SPCT) on ballast particles	
7	DEM simulation of SPCT	
8	Model calibration to obtain calibrated model parameters	
9	Cyclic loading on ballast layer comprising complex-shaped particles simulated using agglomerates of spheres	
10	Document and disseminate the results	
11	Study the permanent deformation behavior of geogrid-reinforced ballast layers and compare results with the non-reinforced ballast layer using simplified ballast particle shapes (using agglomerates of spheres)	Manuscript #3
12	Study the effect of geogrid aperture shape (square vs. triangular) on ballast permanent deformation behavior	
13	Document and disseminate the results	

Organization of the Thesis

This Master's thesis document comprises five chapters.

Chapter 2 contains results reported in the first manuscript published in the Proceedings of the 2018 Joint Rail Conference. The title of the manuscript was, "Simulating Ballast Breakage under Repeated Loading using the Discrete Element Method". This chapter summarizes the research efforts undertaken to understand the significance of ballast breakage considerations on permanent deformation behavior of railroad ballast layer under repeated loading. Various factors that affect the extent of ballast breakage like number of cycles of train loading, magnitude of applied vertical cyclic stress and loading frequency as well as the particle size distribution and micromechanical bond

strength parameters have been individually studied and their effects on the permanent deformation and ballast breakage have been analyzed.

Chapter 3 contain findings reported in a manuscript prepared for submission to the Journal of Computers and Geotechnics. The title of the manuscript is: “Approximating polyhedral ballast shapes using agglomerates of spheres to study ballast layer response under train loading”. This manuscript details improvements over the first manuscript whereby polyhedral particles were approximated using multiple spheres to represent realistic ballast shapes. The information on how the ballast shapes were simulated as well as the laboratory single particle crushing test and eventual crushing strength calibration of the discrete element parameters have been discussed. Subsequently, ballast layer response under repeated loading was simulated using the complex-shaped particle geometries; inferences were draws about the effect of different factors on ballast permanent deformation.

Chapter 4 includes results reported in the third manuscript that has been accepted for publication in the Proceedings of the 2019 Geosynthetics Conference. The title of the manuscript is “Effect of Geogrid Inclusion on Ballast Breakage-A Numerical Study using the Discrete Element Method”. This chapter reports results from the simulations focusing on the interaction between geogrids and ballast particles at a micromechanical level. Findings associated with permanent deformation accumulation and ballast breakage under repeated loading for geogrid-reinforced and unreinforced ballast layers have been reported. The effect of geogrid aperture shape (square vs. triangular) on ballast breakage and permanent deformation accumulation has also been discussed.

Chapter 5 summarizes important findings from this study, and provides recommendations for future research tasks.

References

American-rails. (2016). http://www.american-rails.com. March 2016.

Anderson, W.F., and Key, A.J. (2000). "Model testing of two-layer railway track ballast". J. Geotech. and Geoenv. Eng; 126, 317–323.

Aursudkij, B., McDowell, G. R., and Collop, A. C. (2009). "Cyclic loading of railway ballast under triaxial conditions and in a railway test facility". Granular Matter 11(6), 391–401

Cundall, P. A. (1971). "A computer model for simulating progressive, large-scale movements in rocky block systems". Proc. Symp. Int. Soc. Mech., Nancy 2, No. 8

Cundall, P. A., and Strack, O. D. L. (1979). "A discrete numerical model for granular assemblies". Géotechnique, 29(1), 47–65.

Cundall, P. A., and Hart, R. D. (1992). "Numerical Modelling of Discontinua". Engineering Computations 9, No. 2, 100-113.

Indraratna, B., Ionescu, D., and Christie, H. (1998). "Shear behavior of railway ballast based on large-scale triaxial tests". J. Geotech. and Geoenv. Eng; 124, 439–449.

Indraratna, B., Thakur, P. K., and Vinod, J. S. (2010). "Experimental and numerical study of railway ballast behavior under cyclic loading". Int. J. Geomech., 10(4), 136–144.

Indraratna, B., and Nimbalkar, S. (2011). "Implications of ballast breakage on ballasted railway track based on numerical modelling". 13th Int. Conf. of Int. Assoc. for Comp. Methods and Advances in Geomecs; p. 1085–1092.

Itasca. (2016). "Particle Flow Code in Three Dimensions – PFC 5.0 Documentation". Itasca Consulting Group, Inc., Minnesota.

Lobo-Guerrero, S., and Vallejo, L. E. (2006). “Discrete element method analysis of railtrack ballast degradation during cyclic loading”. J. Granular Matter 8: 195–204. © Springer-Verlag.

Mahmud, S.M. (2017). “Effect of particle size distribution and packing characteristics on railroad ballast shear strength: a numerical study using the discrete element method”. M.S. Thesis, Boise State University, Boise, Idaho, USA

Mishra, D., Tutumluer, E., Boler, H., Hyslip, J., and Sussmann, T. (2014). “Railroad track transitions with multidepth deflectometers and strain gauges”. Transportation Research Record: Journal of the Transportation Research Board, (2448), 105-114.

Neff, J., and Dickens, M. (2013). “Public Transportation Fact Book”. American Public Transportation Association.

Ostria, S.J. (2004). “2010 and Beyond: A Vision of America's Transportation Future: 21st Century Freight Mobility”. ICF Consulting, NCHRP Project 20-24(33) A, August 2004.

Potyondy, D.O., and Cundall, P. A., (2004). “A bonded-particle model for rock”. Int. Journal of Rock Mechanics and Mining Sciences 41, 1329–1364.

Potyondy, D.O. (2015). “The Bonded-Particle Model as a Tool for Rock Mechanics Research and Application: Current Trends and Future Directions”. Geosystem Engineering, 18(1), 1-28.

Saussine, G., Azéma, E., Gautier, P.E., Peyroux, R., and Radjaï, F. (2008). “Numerical modeling of the tamping operation by Discrete Element Approach”. World Congress Rail Research, 1-9.

Selig, E.T., and Waters, J.M. (1994). “Track geotechnology and substructure management”. Thomas Telford Publications 1994, London.

Shenton, M. J., (1975). “Deformation of railway ballast under repeated loading conditions”. Railroad Track Mechanics and Technology (Kerred.), Princeton University, 387–404.

Wright, S. E. (1983). “Damage caused to ballast by mechanical maintenance techniques”. British Rail Research Technical Memorandum TM TD 15, May 1983.

CHAPTER 2: SIMULATING BALLAST BREAKAGE UNDER REPEATED LOADING USING THE DISCRETE ELEMENT METHOD[1]

Abstract

The ballast layer in a railroad track helps distribute loads from the superstructure to the formation; a well-designed ballast layer is also meant to prevent excessive vertical, lateral and longitudinal movement of the track under loading. When subjected to repeated loading, the granular ballast particles often undergo breakage leading to significant changes in the shear strength as well as drainage characteristics of the ballast layer. Excessive ballast degradation leads to increased vertical settlements, and is often associated with speed restrictions and increased passenger discomfort. Several researchers in the past have studied the phenomenon of ballast breakage in a laboratory setting. However, due to complexities associated with these large-scale laboratory tests, detailed parametric studies are often not feasible. In such cases, numerical modeling tools such as the Discrete Element Method (DEM) become particularly useful. This paper presents findings from an ongoing research effort at Boise State University aimed at studying the phenomenon of ballast breakage under repeated loading using a commercially available Discrete Element Package (PFC3D®). Ballast particles were simulated as clusters of balls bonded together, and were

[1] This chapter includes results already reported in the following publication. Contribution of the coauthors is sincerely acknowledged:

Dahal, B., Mahmud, S. N. M., and Mishra, D. (2018). "Simulating ballast breakage under repeated loading using the discrete element method". Proceedings of the 2018 Joint Rail Conference, April 18-21, 2018, Pittsburgh, PA.

allowed to undergo breakage when either the maximum tensile stress or the maximum shear stress exceeded the corresponding bond strength value. Different factors studied during the parametric analysis were: (1) load amplitude; (2) loading frequency; (3) number of cycles of loading; (4) bond strength; and (5) particle size distribution. The objective was to identify the relative importance of different factors that govern the permanent deformation behavior of railroad tracks under loading.

Introduction

The stability and performance of a conventional railroad track system is greatly dependent on behavior of the ballast layer under loading. The ballast layer comprises relatively large (often as large as 63 mm) angular particles that mainly function to transfer the train-induced pressures from ties to the subgrade soils, provide rapid drainage and smooth riding comfort (Selig and Waters, 1994). Under train-induced repeated loading, the ballast particles undergo breakage which gradually deteriorates the quality of the ballast layer, and ultimately leads to speed restrictions, poor drainage, and rapid deterioration in track geometry. This phenomenon of ballast quality degradation due to increased amounts of fines particles, is known as “ballast fouling”. Most of the fouling fines have been reported to originate from ballast breakdown, and the maintenance costs related to the ballast performance have been found to be very high (Lobo-Guerrero and Vallejo, 2006; Indraratna et al., 1998). Ballast breakage in the extreme case may also lead to derailment; this is primarily because vertical settlement of the track mostly occurs in the ballast layer (Selig and Waters, 1994).

Various laboratory as well as field experiments have been conducted to understand the significance of particle crushing or breakage on the permanent deformation (PD)

behavior of the ballast layer (Selig and Waters, 1994; Indraratna et al., 1998; Indraratna et al., 2010a; Aursudkij et al., 2009; Shenton, 1975; Lackenby et al., 2007). Although laboratory and full-scale testing efforts are capable of closely simulating actual field conditions, it is often difficult to fully isolate the effects of individual variables during such efforts. Moreover, extensive parametric studies using laboratory or full-scale set-ups can be prohibitively expensive, and require significant amounts of time to complete, thus rendering such efforts impractical. These experiments also cannot provide a complete picture regarding the evolution of ballast breakage (Indraratna et al., 2010). In order to explore the response of ballast, it is important to simulate ballast using the Discrete Element Method (DEM) as it considers the particulate nature of the matter giving a better representation of the ballast response under loading. Even though these numerical simulations tend to idealize the shape of the particles and their interactions, they can be used to study where the degradation starts, how it evolves, and how it affects the PD of railroad tracks (Lobo-Guerrero and Vallejo, 2006). For this reason, several researchers (Lobo-Guerrero and Vallejo, 2006; Indraratna et al., 1998; Indraratna et al., 2010a; Shenton, 1975; Lackenby et al., 2007) have used DEM simulations to understand the mechanism of ballast layer deformation and degradation during cyclic loading. The ballast particles derive their strength based on the particle interlock mechanism. Hence the response of ballast layer under loading is complex and depends upon various factors like confining pressure (Lackenby et al., 2007), particle size distribution (Indraratna et al., 2006), stress history (Suiker et al., 2005), frequency of loading (Sun et al., 2015), loading conditions (cyclic or static), etc. Moreover, depending on whether individual particles undergo breakage or not, the response under loading of ballast layers can change

significantly. Thorough understanding of these factors and their effects on the ballast breakage response can facilitate the design and construction of better-performing track structures.

Objective of Study

The primary objective of this research effort was to understand the significance of ballast breakage considerations on the Permanent Deformation (PD) behavior of railroad ballast under repeated loading. The extent of ballast breakage is a function of the number of load cycles, applied vertical cyclic stress magnitude, and the loading frequency. It also depends on particle size distribution within the ballast layer, as well as micromechanical parameters such as the nature of inter-particle contact. Parametric studies were conducted to quantify the effects of these factors on ballast breakage; subsequently, the effects on PD behavior of the ballast layer have been analyzed.

Numerical Simulation Using DEM

Modeling Procedure

A 3-D quarter-track model of dimensions 405 mm x 600 mm x 150 mm was created using PFC3D®. Ellipsoidal clumps of ballasts, each comprising 5 balls, were created using the Bubble Pack algorithm within PFC. These clumps were subsequently distributed in the model using a random number generator. Figure 2-1-a shows the particle size distribution curve used for the simulation; a total of 1216 clumps, each comprising five balls, were used in the model. Figure 2-1-b shows the initial assembly of the system after clump generation. In this study, a particle size distribution similar to that used by Indraratna et al. (2010a) was used; the particle sizes were varied between 15 mm and 50 mm. To ensure a reasonably tight initial packing, the overall cloud porosity in the vessel was initially set to 35%. Note

that a similar porosity value was recommended by Potyondy and Cundall (2004) for tight packing in 3-dimensional models. This method of clump distribution in PFC allows large particle overlaps, thereby leading to very high magnitudes of initial stresses; the system was therefore cycled for 50,000 cycles after clump generation to reduce the magnitude of locked-in forces and bring down the mean stress of the system close to zero (a value of 223 Pa was achieved in this case; note that achieving lower values would be possible, but would require significantly higher computational times). The mean stress of the system decreases with the number of DEM time-steps and is asymptotic with a value of ~223 Pa at the end of 50,000 cycles. During this process, the inter-particle friction (pebbles-pebble, pebble-facet) was set to zero to obtain the maximum packing density. The values of different model parameters used in this study have been listed in Table 2-1. The wall normal and shear stiffnesses were set to twice the average particle normal and shear stiffnesses, respectively, to ensure that the particle–wall overlap remains small (Potyondy and Cundall, 2004; Potyondy, 2015). Finally, the desired packing friction and density values were assigned to the particles in the system.

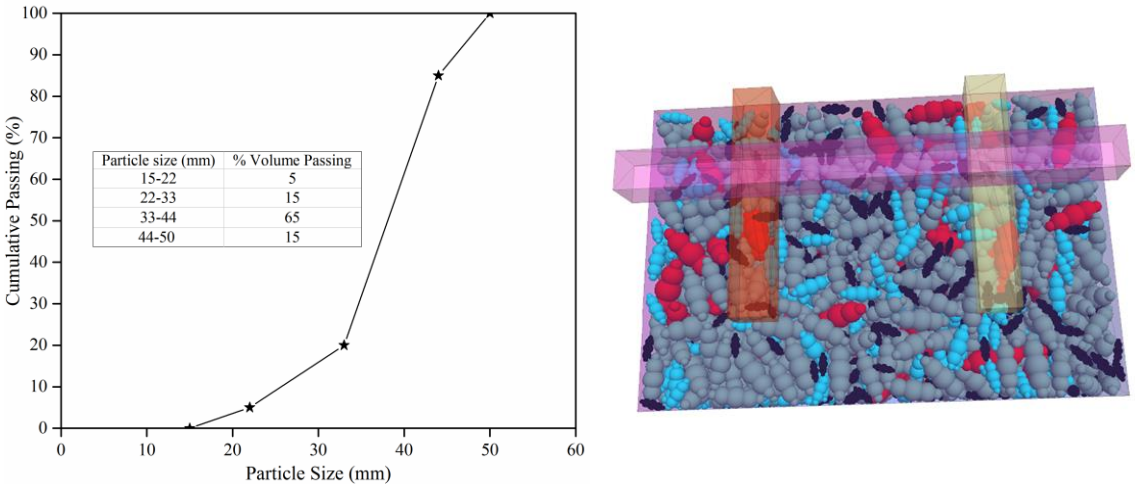

(a) (b)

Figure 2-1: (a) Particle Size Distribution of Ballast used in the Simulation; (b) Specimen Box with Clumps (Dahal et al., 2018)

Indraratna et al. (2010b) mention that confinement provided by the crossties, shoulder ballast, and crib ballast results in a mean confining stress value between 10-60 kPa (1.4-8.7 psi) within the ballast layer. Considering its relatively small magnitude, this initial confining pressure was not included in the current modeling effort. Therefore, after clump generation, the system was applied with the mean stress of cyclic loading of 232 kPa (similar to Indraratna et al. (2010a)) through the wall servo mechanism applied via top wall of the specimen box. The set of ties and rails shown in the Figure 2-1-b are modelled only to help readers understand the real configuration of the track as in this simulation, load on the ballast layer was applied through the entire top wall not through the ties and rails.

Table 2-1: Parameters used in DEM Simulations

Model Parameters	Values
Specimen Size	Length = 405 mm; Width = 600 mm; Height = 150 mm
Particle density	2500 kg/m^3
Damping ratio	0.7
Inter-particle and wall friction	0.25
Particle normal and shear contact stiffness (k_n, k_s)	3x10^8 N/m
Wall stiffness (k_n, k_s)	6x10^8 N/m
Acceleration due to gravity	9.81 m/s^2
Parallel bond normal and shear stiffness ($\overline{k_n}$, $\overline{k_s}$)	6x10^{10} N/m^3
Parallel bond normal and shear strength (σ, τ)	3x10^7 N/m^2
Parallel bond radius multiplier ($\bar{\lambda}$)	0.5

Application of Repeated Loading

A subroutine was created to apply the cyclic or repeated load to the top wall and monitor the permanent deformation of the ballast layer. The sinusoidal load was cycled between two compressive stress states of q_{min} and q_{max}. The maximum cyclic stress (q_{max}) is the magnitude of the cyclic loading which depends on the maximum rail seat load (Sun et al., 2015). The minimum cyclic stress (q_{min}) value represents the in-situ ballast layer pressures in the unloaded state of the track and can be attributed to the static weight of the sleepers and rails (Lackenby et al., 2007). The sinusoidal load in this simulation varied between q_{min} of 45 kPa and q_{max} of 419 kPa. These values were obtained from the research effort reported by Indraratna et al. (2010a). The mean cyclic loading stress was set to 232 kPa. The frequency of the cyclic loading was set to 10 Hz, and the amplitude was 187 kPa. This load was applied till 50 cycles for the breakable specimen and the stress-strain response of the ballast sample was plotted.

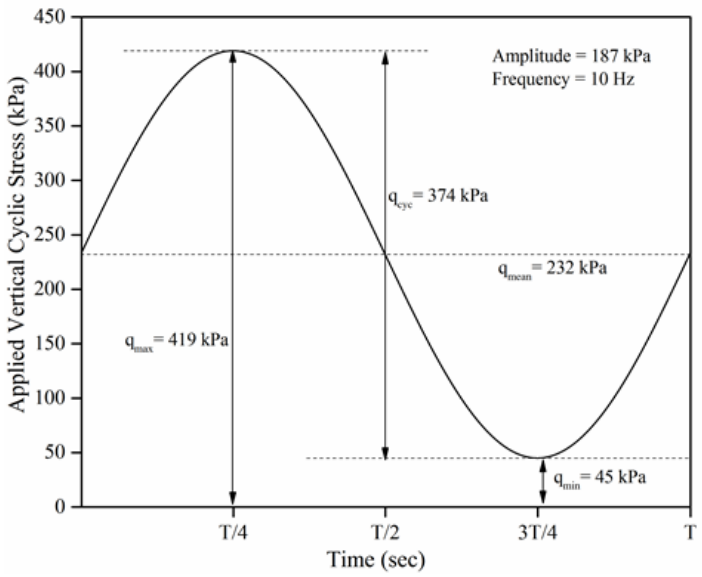

Figure 2-2: Typical Cyclic Loading Curve used in Numerical Simulation (Dahal et al., 2018)

Stress was taken as the ratio of the load experienced by the top wall to the area of the top wall. Strain was calculated using the relative distance between the top and the bottom walls after loading divided by the initial distance between the walls. The values of PD as a function of number of cycles and also the number of breakages were also recorded. Two types of simulations were carried out: one allowed particle breakage, whereas the other did not allow particle breakage. For the non-breakable specimen, the system was cycled until 200 cycles. Figure 2-2 shows the typical loading curve used during this research effort to simulate the repeated or cyclic loading on the ballast specimen.

Particle Breakage Criteria

Researchers in the past have used different approaches to model particle breakage in DEM simulations using PFC. Lobo Guerrero and Vallejo (2006) and Hossain et al. (2007) simulated breakage using an approach whereby a particle on meeting a designated failure criterion was replaced with an equivalent combination of small rounded particles of

different sizes. Indraratna et al. (2010a) simulated particle breakage by first releasing the clumps and then installing parallel bonds between individual particles within the clumps to represent the breakable particles; on meeting a predefined failure criterion, these bonds would break resulting in multiple unbonded particles. The current modeling effort used an approach similar to that used by Indraratna et al. (2010a); clumps were first disaggregated to form clusters, and Linear-Parallel bonds (detailed description provided below) were installed at the ball-ball contacts inside each cluster. These bonded particles would separate when the stresses in the bond exceed the predefined strength values. Note that the bond strengths assigned to the clusters in this manuscript (primary factor governing particle breakage) were modified from values reported in the literature; realistic simulation of ballast breakage phenomenon should utilize single particle crushing strength data obtained from laboratory testing. The authors are currently working on obtaining such data, and corresponding results will be published in future manuscripts.

A Linear-Parallel (LP) bond exhibits the mechanical behavior of a group of grains joined together by brittle elastic cement (Potyondy and Cundall, 2004; Potyondy, 2015). The LP bond model consists of a grain-based portion and parallel bond portion represented by a set of elastic springs that act in parallel with each other. Figure 2-3 represents the rheological behavior of a linear-parallel bond model with inactive dashpots in PFC (Itasca, 2016). These elastic springs lie on the contact plane and are centered at the contact point. The parallel bond springs are uniformly distributed over a rectangular cross-section in PFC2D, and a circular cross-section PFC3D respectively (Potyondy and Cundall, 2004; Potyondy, 2015). They behave like beam whose length approaches zero at the contact representing mechanical behavior of a joint. These bonds can transmit both moment as well

as force between particles acting like a cement connecting two pieces that provide rotational resistance. In PFC, five micromechanical parameters define the parallel bond properties: normal and shear stiffnesses per unit area ($\overline{k_n}, \overline{k_s}$); tensile and shear strengths (σ, τ), and bond-radius multiplier ($\bar{\lambda}$). When the load is applied to the assembly of parallel bonded particles, disturbance is created in the specimen and hence the particles move around causing the parallel bonds to develop force and moments within the bonds. The maximum tensile and shear stresses that can act on the periphery of the parallel bond are given by the following two equations.

$$\sigma_{max} = \frac{-F^n}{A'} + \frac{|M^s|}{I} R \qquad (1)$$

$$\tau_{max} = \frac{|F^s|}{A'} + \frac{|M^n|}{J} R \qquad (2)$$

where σ_{max} and τ_{max} represent the maximum tensile and shear stresses acting on the periphery of the bond; A', J and I represent the area, the polar moment of inertia, and the moment of inertia of the cross section of the parallel bond, respectively; F^n and F^s and M^n and M^s are axial and shear directed forces and moments carried by the bond; and R represents the radius of the bond. When the maximum tensile stress or maximum shear stress exceed the tensile strength or the shear strength respectively, the parallel bond breaks and is removed from the model along with its accompanying force, moment and stiffnesses (Potyondy and Cundall, 2004; Potyondy, 2015). As can be observed from Figure 2-3, in this unbonded state, only the linear contact model is present which actually represent the unbonded group of grains.

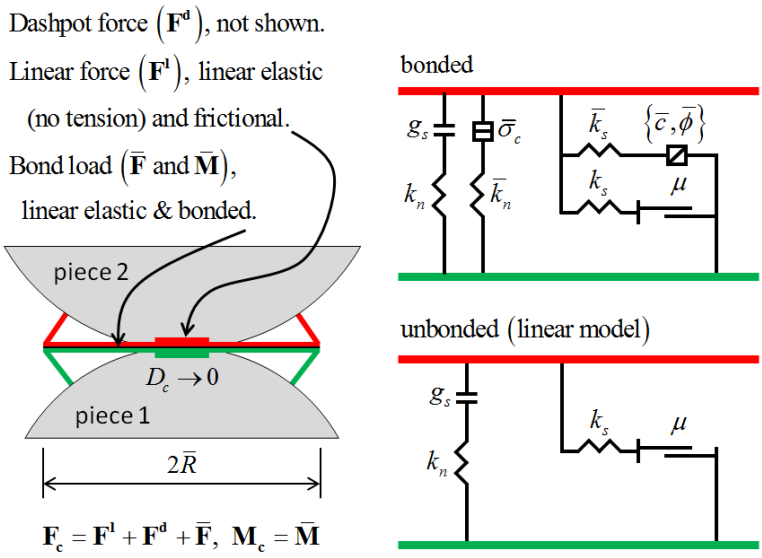

Figure 2-3: Behavior of Linear Parallel Bond Model with Inactive Dashpots (Itasca, 2016)

Simulation of Ballast Breakage

After the application of initial stress and before the application of sinusoidal or repeated load, to simulate granulation, clumps were replaced with clusters of balls. In this process, the clumps were released and replaced with balls with the same radius as the pebbles constituting the clumps. Subsequently, the balls within each cluster (previously clumps) were bonded together using LP bonds. These bonds were assigned bond properties of normal and shear bond stiffnesses and tensile and cohesion strengths along with the parallel bond radius multiplier as tabulated in Table 1. Note that concept of radius multiplier has been discussed later in this manuscript. The values k_n and k_s were set equal as the $\frac{\bar{k}_n}{\bar{k}_s}$ ratio does not significantly affect the compressive strength created by bonded particles (Yang et al., 2006). The new contacts that form in between the clusters were assigned the default contact of linear contact model. Breakage of the bonds within the balls in each cluster was considered as particle breakage. Once there was breakage in the cluster,

the size of the cluster was updated, and contact properties between the broken particles were assigned as linear bond. This simulation did not restrict the updated smaller particles from breaking and the breakage was allowed until a single particle was left of each cluster.

Results and Discussions

Figure 2-4-a and Figure 2-4-b show the LP bonds (represented as cylinders) in the ballast layer before and after application of the sinusoidal load. As clearly seen, the number of bonds after load application (Figure 2-4-b) is less than that before load application (Figure 2-4-a). The number of linear parallel bonds before and after the application of load was 4864 and 4706, respectively. This is direct evidence of bond breakage under loading.

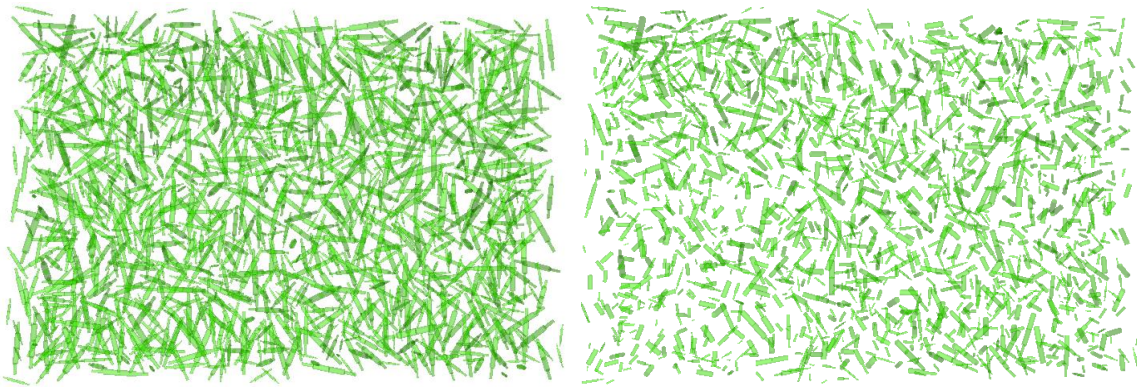

(a) (b)

Figure 2-4: Linear Parallel Bonds in the Clusters (a) Before Breakage; (b) After Breakage (Dahal et al., 2018)

Figure 2-5-a shows the applied vertical cyclic stress- vertical axial strain response of the ballast specimen under the applied sinusoidal load. As seen from the figure, the axial strain accumulation after the first load cycle is significantly higher than that after successive load cycles (the permanent strain accumulation after the first load cycle equaled 2%). The rate of permanent strain accumulation gradually decreased for subsequent cycles, with the recoverable (or resilient) component of axial strain accounting for a major

component of the total deformation per load cycle; a near-complete hysteretic behavior was reached after approximately 50 load cycles (indicative of primarily resilient behavior). The number of bond breakage was highest during the initial load cycles, and gradually decreases during subsequent cycles. For instance, there were a total of 158 bond breakages (after 50 cycles) observed during the simulation. Out of these, 65 bonds broke during the 1st load cycle. The total number of bond breakages reached 103 within the first 10 load cycles; the rate of bond breakage per load cycle reduced thereafter. Looking at the PD curve as well, it shows similar trends (high PD accumulation during initial load cycles). Therefore, it can be safely said that the high rate of PD accumulation during initial cycles for the model with breakable ballast clumps was primarily due to breakage of individual particles. Note that similar trends were reported by Indraratna et al. (2010a).

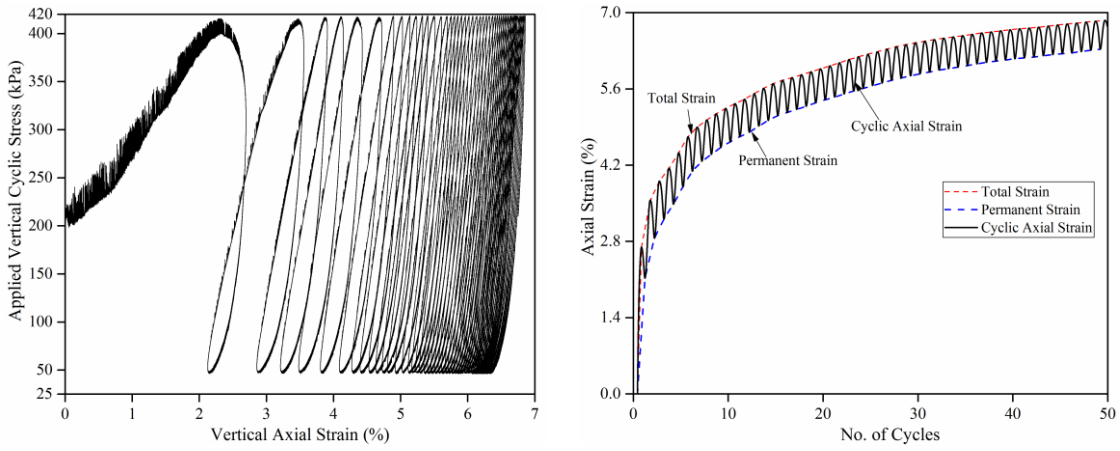

Figure 2-5: (a) Applied Vertical Cyclic Stress vs Vertical Axial Strain Response of Ballast Specimen under Repeated Loading; (b) Vertical Strain Accumulation with Number of Load Cycles for the Model Comprising Breakable Ballast (Dahal et al., 2018)

Figure 2-5-b shows the results of evolution of axial strain as a function of number of load cycles for a test configuration with breakable ballast clumps. The permanent as well as resilient components of axial strain can be extracted from this figure. As seen from the

figure, the total axial strain after the first load cycle was very high (*~2.6%*), with most of this strain coming from the permanent/plastic strain component. During subsequent load applications, the total strain increases at a decreasing rate; the contribution of the permanent strain component towards total strain per cycle reduces, whereas contribution of the recoverable (resilient) component increases. The strain started to stabilize after 40 cycles, but it will take more cycles to completely stabilize the specimen or have consistent PD values. The simulation was stopped after 50 cycles as some of the stabilization was already observed. At the end of 50 cycles, the PD of the ballast was found to be 9.97 mm.

Similar trends were observed for the model comprising non-breakable ballast clumps. The total permanent deformation accumulation after 200 cycles was 2.29 (compared to 9.97 mm after 50 cycles for the model with breakable ballast clumps). Lobo Guerrero and Vallejo (2006) also reported lower PD values for specimens with non-breakable particles compared to those with breakable particles. Note that the model comprising non-breakable ballast particles did not attain primarily resilient behavior under 50 loading cycles, and therefore, more load cycles were applied to ensure the model attained a "stable" state. Accordingly, during the parametric analysis, the model with non-breakable ballast clumps was tested to 200 load cycles. Note that even after the application of 200 load cycles, non-zero permanent deformation accumulation per load cycle was observed, indicating a state where the ballast response was not primarily resilient in nature. However, the simulations were terminated after 200 cycles to save computational times.

As already mentioned, the ballast clumps used in this simulation effort were primarily ellipsoid in nature, which marks a significant deviation from the real-world scenario, where particles are mostly polyhedral. To ensure that the assumption of

ellipsoidal particles does not adversely affect the simulation results, a verification effort was carried out by analyzing the same model with polyhedral-shaped ballast particles. This polyhedral particle template was prepared to match realistic ballast particle shapes, and the clump was generated using 18 pebbles of different sizes. Figure 2-6 compares the vertical strain accumulation with number of load cycles for the model comprising polyhedral-shaped clumps to that for the model comprising ellipsoid-clumps (both clumps were modeled as non-breakable). As seen from the figure, no significant difference between the two models was observed as far as axial strain accumulation trends were concerned. Taking this as a reference, subsequent simulation efforts were carried out using the simple ellipsoid ballast clumps as it was easier to apply bonds between the pebbles in the ellipsoid for simulating particle breakage.

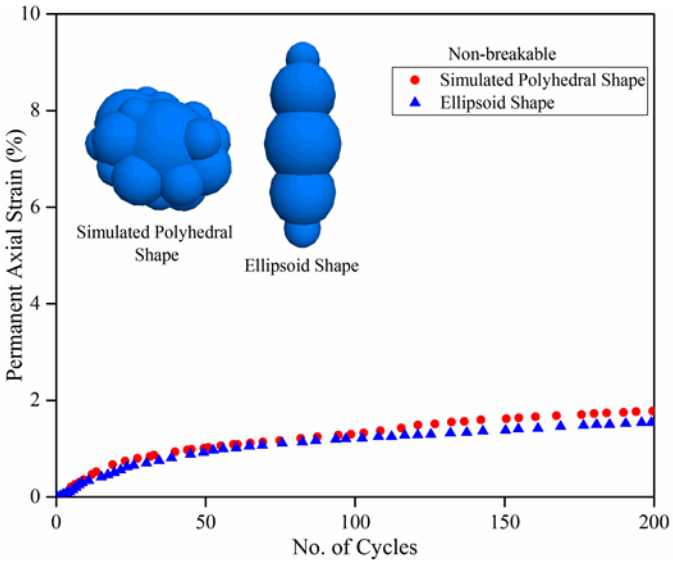

Figure 2-6: Vertical Strain Accumulation with Number of Load Cycles for Polyhedral- and Ellipsoid-Shaped Non-Breakable Clumps (Dahal et al., 2018)

Results from parametric analyses conducted to study the effects of different loading and micromechanical parameters on ballast breakage and permanent deformation behavior have been presented in the following sections.

Effect of Number of Cycles

The number of load cycles can be directly correlated to the volume of train traffic that a track structure is subjected to. Considering that ballast breakage and the resulting permanent deformation accumulation have been found to be significant factors affecting overall track geometry, a good understanding of the effect of number of load cycles on ballast breakage and PD behavior is important. During the current simulation effort, behavior of the ballast layer was compared for both breakable as well as non-breakable particles after 10, 50, and 200 load applications, and the results have been plotted in Figure 2-7. As seen from the figure, the permanent strain accumulation increased rapidly during the initial cycles of loading, and the rate of PD accumulation per cycle gradually reduced to approximate primarily resilient behavior; similar results were reported by Indraratna et al. (2010a). This trend was observed for both the breakable and non-breakable ballast clumps. Table 2-2 lists the effect of number of load cycles on ballast breakage and PD accumulation. The ballast breakage is also the highest for the initial 10 cycles after which the rate of increase of ballast breakage is not as high. Once the bond breakage tended to cease with increasing number of load cycles, the rate of permanent deformation accumulation per cycle also decreased.

The total permanent deformation accumulation for non-breakable ballast clumps after 10, 50 and 200 cycles were 0.47 mm, 1.38 mm and 2.29 mm, respectively. This strain accumulation could be primarily due to the densification of ballasts through particle

rearrangement with increasing number of load applications. From Figure 2-7, on comparing the plots for breakable and non-breakable ballast clumps, it can be seen that at the end of 200 cycles, the PD for the model with breakable ballast particles was more than 400% of that for the model with non-breakable ballast particles. Therefore, treating ballast particles as non-breakable during DEM simulations can significantly underestimate the vertical strain accumulations. Ballast breakage consideration directly affects the permanent strain accumulation which initially increases with increasing number of load cycles, and later attains an asymptotic value as the ballast response becomes more and more resilient.

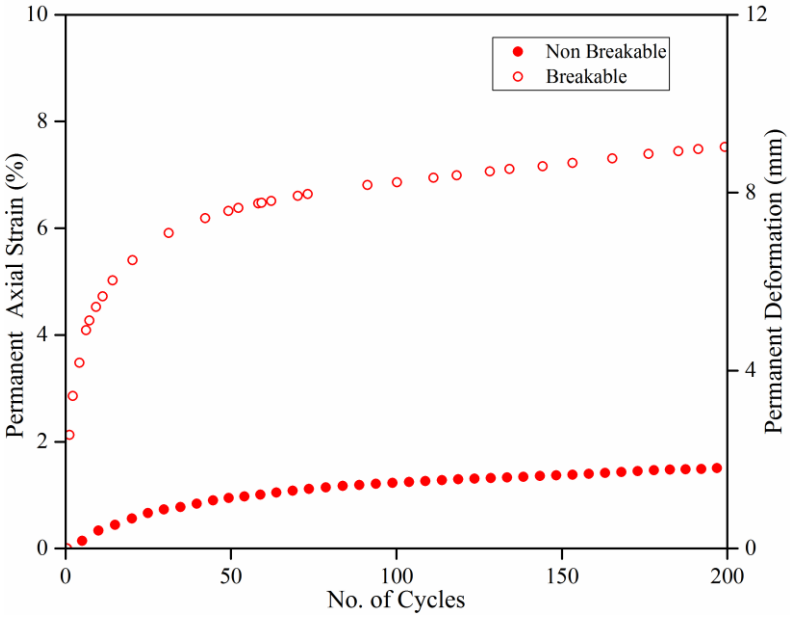

Figure 2-7: Vertical Strain and PD Accumulation with Number of Load Cycles for Breakable and Non-breakable Ballast Clumps (Dahal et al., 2018)

Table 2-2: Effect of Number of Load Cycles on Ballast Breakage and PD Accumulation (Results for the Model Comprising Breakable Ballast Clumps)

Number of Cycles	No. of Breakage	PD (mm)
10	103	7.47
50	158	9.97
200	177	11.80

Effect of Load Amplitude

Axle load magnitudes, combined with the width and length of ties can significantly affect the stresses transmitted to the ballast layer (Indraratna et al., 2010a). Researchers in the past (Olowokere, 1975; Knuston, 1976) have reported increased permanent deformation magnitudes with increasing applied cyclic stress levels. Under low amplitude of cyclic loading, the ballast layer tends to densify, thus leading to increased strength and stiffness (Indraratna and Salim, 2005).

The effect of load amplitude on ballast breakage and PD response was studied in the current research effort under three different stress levels: 100kPa, 187kPa and 300kPa. The subroutine created to apply the sinusoidal stress was designed such that the amplitude would vary based on the initial mean stress of cyclic loading applied, and the cyclic load would vary about this mean stress value. Accordingly, for each different target load amplitude, the initial mean stress magnitude was varied; the initial mean stress values for target load amplitude values of 100 kPa, 187 kPa, and 300 kPa were set to 145 kPa, 232 kPa and 345 kPa respectively. This ensured that the q_{min} value of 45 kPa was maintained for all cases. Note that a similar approach was reported by Indraratna et al. (2010a). Figure 2-8 shows the variation of PD with number of cycles for different stress amplitudes for the models comprising breakable as well as non-breakable clumps. As the load amplitude was increased from 100 kPa to 300 kPa, the PD value increased significantly, particularly for the model comprising breakable ballast particles. Sun et al. (2015) also observed this trend of increasing PD with increasing cyclic stress amplitude. Table 2-3 lists the number of breakages observed for each applied load amplitude.

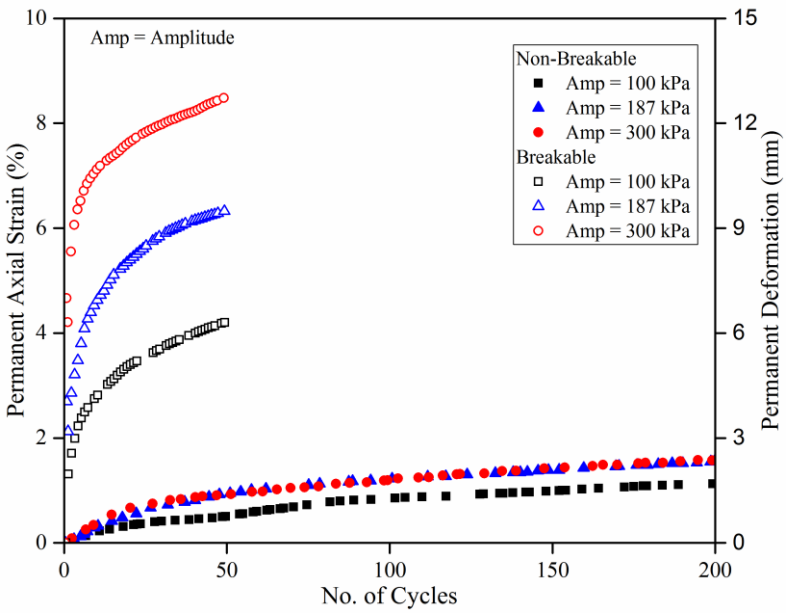

Figure 2-8: Vertical Strain and PD Accumulation with Number of Load Cycles with varying Amplitudes for Breakable and Non-Breakable Ballast Clumps (Dahal et al., 2018)

Table 2-3: Effect of Stress Amplitude on Ballast Breakage and PD Accumulation after 50 Load Cycles (Results for the Model Comprising Breakable Ballast Clumps)

Amplitude (kPa)	Initial Stress (kPa)	No. of Breakage	Permanent deformation (mm)
100	145	44	6.74
187	232	158	9.97
300	345	440	12.86

As expected, the number of bond breakage increases significantly as the load amplitude increases. The PD accumulation for the model with non-breakable ballast particles was significantly lower than the model with breakable ballast particles; after 200 load cycles, the PD values corresponding to 100 kPa, 187 kPa, and 300 kPa load magnitudes were 1.68 mm, 2.29 mm and 2.34 mm, respectively. Interestingly, no significant increase in PD accumulation with load amplitude was observed for the model with non-breakable ballast particles. This can be attributed to the increased mean-stress levels applied for increased load amplitude cases. As the mean-stress magnitude increases,

the ballast is in a better-confined state, and therefore, the resistance to permanent deformation increases significantly. This effect of increased confining stress gets negated in case of breakable ballast particles, and the PD accumulation increases due to excessive breakage of bonds.

Effect of Loading Frequency

Various research studies have been performed to understand the significance of train speed on ballast breakage and PD response of the ballast layer. Load frequency is a function of train speed and the characteristics length between the closest sets of axles (Knuston, 1976). Therefore, the value of frequency varies with the speed of the train. The effect of frequency of cyclic loading on PD has been found to be contradictory based on different studies. Shenton (1975) studied the effect of frequency on ballast and found that frequency values within the range of 0.1 Hz to 30 Hz do not have significant influence on the PD in the ballast samples. Indraratna et al. (2010a), observed a clear dependency of cyclic loading frequency on ballast PD; increased permanent deformation and ballast breakage were reported with increasing loading frequency.

During the current research effort, the effect of loading frequency on ballast breakage and PD response was studied using three different frequency levels: 5 Hz, 10 Hz and 50 Hz. The PD as well as particle breakage were found to decrease with increasing loading frequency when the simulation was run for 50 cycles for both the breakable and non-breakable ballast clumps. Researcher in the past have reported that for higher frequency values, higher number of load cycles are required to stabilize the axial strain (Indraratna et al., 2010a). Accordingly, the simulations in this study were run for 200 cycles for both the breakable and non-breakable ballast clumps.

Figure 2-9 shows the vertical strain as well as PD accumulation with number of load cycles for varying loading frequencies. It can be seen that for both the breakable and non-breakable ballast clumps cases, there is a very slight difference in the permanent deformation values for different loading frequencies after 200 loading cycles. Although the rate of PD accumulation for the lowest frequency (5 Hz) was significantly higher than that for the highest frequency (50 Hz) during the initial load cycles, total PD magnitude after 200 cycles were similar for all three frequency values. The PD values for the model with non-breakable clumps after 200 cycles were found to be 2.38, 2.29 and 1.81 mm for 5 Hz, 10 Hz, and 50 Hz loading frequencies, respectively. Table 2-4 lists the number of bond breakage (after 200 Cycles) and PD for 50 cycles and 200 cycles of applied cyclic loading. From these results, it appears that loading frequency does not have significant effect on the PD accumulation when large number of load cycles are considered.

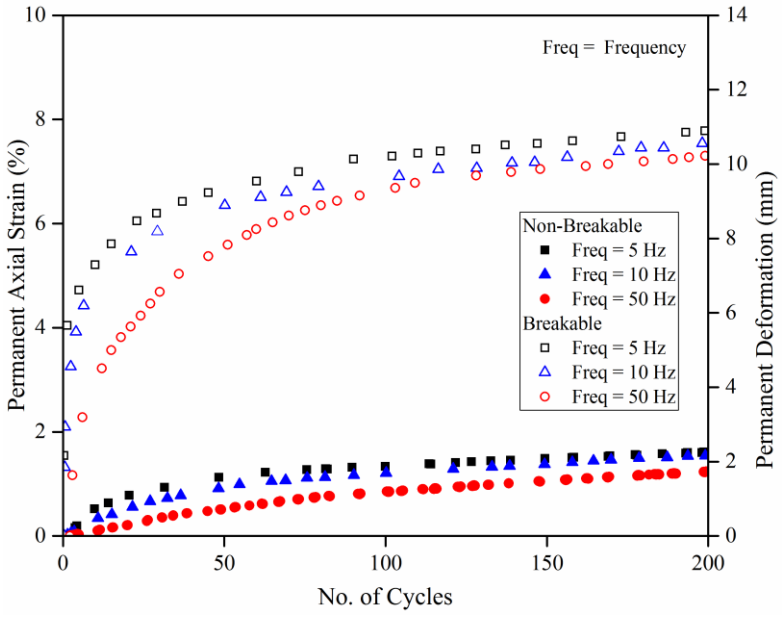

Figure 2-9: Vertical Strain and PD Accumulation with Number of Load Cycles with varying Frequencies for Breakable and Non-breakable Ballast Clumps (Dahal et al., 2018)

Table 2-4: Effect of Frequency on Ballast Breakage (@200 cycles) and PD Accumulation (@50 and @200 cycles) (Results for the Model Comprising Breakable Ballast Clumps)

Frequency (Hz)	No. of Breakage (200 cycles)	PD (50cycles) (mm)	PD (200 cycles) (mm)
5	218	9.88	11.92
10	177	9.97	11.80
50	160	8.19	11.05

Effect of Bond Strength

According to Indraratna and Salim (2005), the parent ballast strength has significant influence on the deformation and degradation of ballast under loading. Accordingly, the shear and tensile bond strength values assigned to the linear parallel bond during discrete element modeling signify the strength of the ballast particles and have a great role in governing ballast breakage and PD accumulation.

To study this behavior during the current research effort, the following three values of parallel bond strengths were used: $1x10^7$ N/m^2, $3x10^7$ N/m^2, and $5x10^7$ N/m^2. Note that the effective bond strength in a PFC model depends on the tensile/shear strengths assigned to the bond, as well as the 'radius multiplier', which determines the area over which the bond is applied. The radius multiplier value used to set the radius of the parallel bond at a particular contact depends on the diameter of the smaller of the two particles in contact, and its value ranges from 0-1. A value of 1.0 assigned to the radius multiplier indicates a larger the bond area; during the current simulation effort, the radius multiplier value was kept constant at 0.5 In other words, the parametric study in this research effort focused primarily on the normal/shear strength of the bond, and not on the area over which the bond is applied at the contact between two particles. The shear and tensile bond strength values were assigned the same magnitude to ensure both tensile and shear micro failures were

possible (Potyondy and Cundall, 2004; Potyondy, 2015). It is important to note that the primary objective of this particular parametric study was to assess how ballast breakage and PD accumulation can be affected by whether individual ballast particles are susceptible to breakage under loading or not. Considering that this study is not validated using actual laboratory test data, the bond strength values used during the simulation effort might not reflect actual ballast particle strengths.

Table 2-5 lists the number of breakage and the PD accumulations when the bond strengths assigned to individual ballast clumps were varied. Figure 2-10 presents the same data in terms of the evolution of PD with number of loading cycles. As expected, with an increase in bond strength, the number of bond breakage as well as the PD reduce significantly. A higher number of bond breakage leads to increased amounts of particle reorientation and volumetric compaction (also referred to as cyclic densification, (Indraratna et al., 2016)), ultimately resulting in higher PD accumulations. This finding can be directly extended to the importance of using mineralogically strong (relatively difficult to break) ballast particles during track construction, compared to ones that would break easily under repeated train loading.

Table 2-5: Effect of Bond Strength on Ballast Breakage and PD Accumulation after 50 Load Cycles (Results for the Model Comprising Breakable Ballast Clumps)

Bond Strength (N/m)	No. of Breakage	PD (mm)
$1x10^7$	2098	22.92
$3x10^7$	158	9.97
$5x10^7$	13	9.04

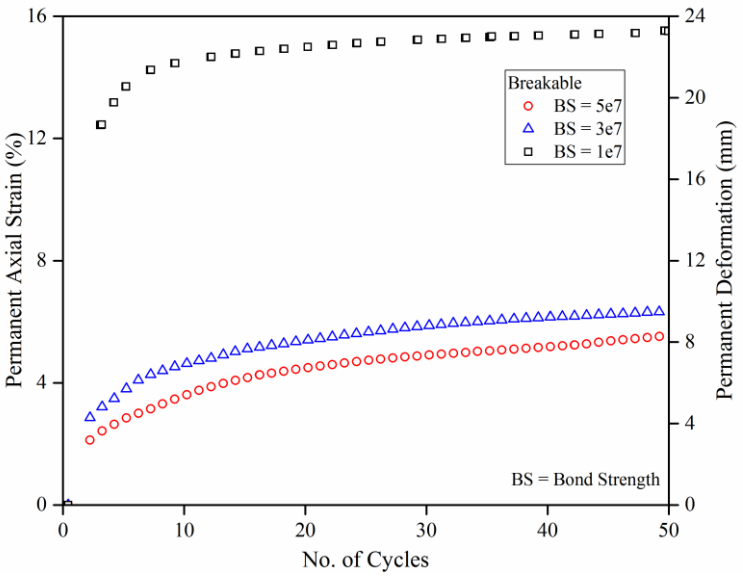

Figure 2-10: Vertical Strain Accumulation and PD with Number of Load Cycles with varying Bond Strength values for Breakable Ballast Clumps (Dahal et al., 2018)

Effect of Particle Size Distribution

The final task in this parametric effort involved studying the effects of particle size distribution on ballast breakage and PD accumulation. Indraratna et al. (2016) observed that the resistance to permanent deformation accumulation in ballast can be reduced by increasing the relative density of the matrix, which is governed by the Particle Size Distribution (PSD). They also reported initial reduction and subsequent increase in permanent axial strain as the Coefficient of Uniformity (C_u) value was changed for the ballast matrix; they proposed an optimum PSD ($1.8 \leq C_u \leq 2.0$) that would exhibit the lowest deformations (Indraratna et al., 2016).

To study the effect of PSD on ballast breakage and PD accumulation, the current simulation effort focused on three different ballast gradations. 'PSD1' refers to the control case as shown in Figure 2-1. 'PSD2' refers to a variation of 'PSD1', where the largest 'bin size' was changed from '44 mm - 50 mm' to '50 mm - 67.5 mm'. 'PSD3', on the other

hand, retained the same top size as 'PSD1', but all particles corresponding to the smallest bin (15 mm – 22 mm) were removed. Figure 2-11 shows the vertical strain accumulation with number of load cycles with varying particle size distribution for both the breakable and non-breakable ballast clumps. For the models comprising non-breakable ballast clumps, the PD values (after 200 load cycles) were 2.29, 1.99 and 1.95 mm, for PSD1, PSD2, and PSD3, respectively. Table 2-6 shows the effect of particle size distribution on the ballast permanent deformation and the number of ballast breakage; C_u values for the different gradations are also listed.

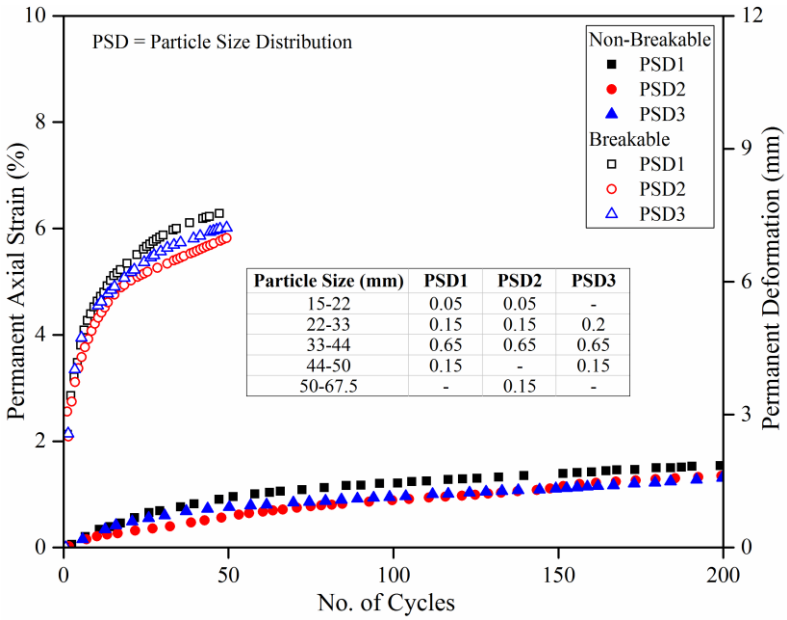

Figure 2-11: Vertical Strain Accumulation and PD with Number of Load Cycles with varying Particle Size Distribution for Breakable and Non-breakable Ballast Clumps (Dahal et al., 2018)

From Figure 2-11, it can be observed that increasing the maximum particle size (i.e. moving from PSD1 to PSD2) led to reduced PD accumulation for both breakable as well as non-breakable ballast particles. Similar observations were reported by Janardhanam and Desai (1983). Moreover, Indraratna et al. (2016) observed that larger aggregates underwent

smaller axial strain under repeated loading, which can be related to improved shear resistance. PSD1 for the breakable particles showed 7.6% and 3.3% more PD than PSD2 and PSD3, respectively. For models with non-breakable clumps, PSD1 showed 15.1% and 17.4% higher PD compared to PSD2 and PSD3, respectively. Based on these results, it can be inferred that changing PSD affects the PD behavior of non-breakable ballast clumps more significantly compared to breakable ballast clumps. As seen from Figure 2-11, for the model with breakable ballast clumps, breakage was the highest for PSD1, and lowest for PSD2 (at the end of 50 load cycles). Based on these results, it can be inferred that increasing the ballast top size or removing the smallest particle size from and original PSD leads to reductions in the number of particle breakage as well as the permanent deformation accumulation under repeated loading.

Table 2-6: Effect of Particle Size Distribution on Ballast Breakage and PD Accumulation after 50 Loading Cycles (Model Comprising Breakable Ballast Clumps)

Name	No. of clusters	No. of Breakage	PD (mm)	C_u
PSD1	1216	158	9.97	2
PSD2	1185	124	9.27	1.98
PSD3	977	137	9.65	1.49

Summary and Conclusions

This manuscript presented results from a discrete element modeling effort aimed at studying the effects of different loading and material parameters on permanent deformation accumulation in the ballast layer of a ballasted railroad track; both breakable and non-breakable ballast particles were considered. The following conclusions can be drawn based on the simulation results.

1. PD accumulation under cyclic loading was significantly higher for the model with breakable ballast particles compared to the one with non-breakable ballast particles.
2. Majority of the deformation and breakage occurred under the first few loading cycles. As the number of loading cycles increased, the percent of breakage as well as the permanent deformation accumulation per cycle decreased.
3. Higher loading magnitudes led to increased particle breakage and PD accumulation.
4. The effect of loading frequency on PD accumulation was found to be greater for models comprising non-breakable ballast particles, compared to the ones with breakable ballast particles. In case of breakable ballast particles, the rate of PD accumulation was higher for low loading frequencies during the initial loading cycles. However, the total accumulated PD magnitude was comparable across different loading frequencies after 200 load cycles.
5. As expected, increased bond strength led to decreased ballast breakage and PD accumulation.
6. Based on the results, it was observed that increasing the ballast top size or removing the lower size, both resulted in the decrease in PD.

Limitations

The simulation effort reported in the current manuscript has the following limitations:

1. The cyclic load magnitudes used in the simulations might not be representative of actual train loads. Using field-measured stress data in the ballast layer can lead to better representation of real-world scenarios;

2. The permanent deformation curves were not completely asymptotic after 50 cycles (for breakable particles) or 200 cycles (for non-breakable particles). However, the simulations were stopped at these points to avoid excessively high computational times;
3. Not all the particles undergo same type of breakage (Lobo-Guerrero and Vallejo, 2006). However, in the current simulation, all the particles undergo same type of breakage i.e. splitting of the LP bonds between balls in the clusters on meeting the failure criteria;
4. The real railroad track contains different shapes of ballast particles. In this study, even though angular particles were used, only a single particle type with simple angular shape was used. Considering different particles shapes within the same model will better replicate actual field conditions;
5. Lateral spreading of the ballast under train load application was not considered in this study.

Acknowledgments

The authors acknowledge the help provided by Dr. David Potyondy and Mr. Derrick Blanksma of Itasca during the discrete element modeling efforts.

References

Aursudkij, B., McDowell, G. R., and Collop, A. C. (2009). “Cyclic loading of railway ballast under triaxial conditions and in a railway test facility”. Granular Matter 11(6), 391–401

Dahal, B., Mahmud, S. N. M., and Mishra, D. (2018). “Simulating ballast breakage under repeated loading using the discrete element method”. Proceedings of the 2018 Joint Rail Conference, April 18-21, 2018, Pittsburgh, PA.

Hossain, Z., Indraratna, B., Darve, F., and Thakur, P. K. (2007). “DEM analysis of angular ballast breakage under cyclic loading”. Geomech. Geoeng.; 2(3), 175–181.

Indraratna, B., Ionescu, D., and Christie, D. (1998). “Shear behavior of railway ballast based on large-scale triaxial tests”. ASCE J. Geotechn. Geoenvron. Eng. 124(5), 439-449

Indraratna, B., and Salim, W. (2005). “Mechanics of ballasted rail tracks-A geotechnical perspective”. Taylor & Francis/Balkema, London.

Indraratna, B., Khabbaz, H., Salim, W., and Christie, D. (2006). “Geotechnical properties of ballast and the role of geosynthetics in rail track stabilisation”, Proceedings of the Institution of Civil Engineers-Ground Improvement, 10(3): 91-101.

Indraratna, B., Thakur, P. K., and Vinod, J. S. (2010a). “Experimental and numerical study of railway ballast behavior under cyclic loading”. Int. J. Geomech., 10(4), 136–144.

Indraratna, B., Nimbalkar, S., Christie, D., Rujikiatkamjorn, C., and Vinod, J. S. (2010b). “Field assessment of the performance of a ballasted rail track with and without geosynthetics”. J. Geotech. Geoenviron. Eng.

Indraratna, B., Biabani, M. M., and Nimbalkar, S. (2015). “Behavior of geocell-reinforced subballast subjected to cyclic loading in plane-strain condition”. J. Geotech. Geoenv. Eng., 10.1061/(ASCE)GT.1943-5606.0001199, 04014081-1-16.

Indraratna, B., Sun, Y., and Nimbalkar, S. (2016). "Laboratory assessment of the role of particle size distribution on the deformation and degradation of ballast under cyclic loading". J. Geotech. Geoenviron. Eng., 142(7): 04016016.

Itasca Consulting Group, Inc. (2016). “PFC - Particle Flow Code”. Ver. 5.0. Minneapolis: Itasca.

Janardhanam, R., and Desai, C. (1983). "Three dimensional testing and modeling of ballast". J. Geotech. Eng., 109(6): 783-796.

Knutson, R. M. (1976). “Factors influencing the repeated load behavior of railway ballast”. Ph. D. Thesis, University of Illinois, at Urbana, Illinois

Lackenby, J., Indraratna, B., McDowell, G., and Christie, D. (2007). “Effect of confining pressure on ballast degradation and deformation under cyclic triaxial loading”. Géotechnique, 57(6), 527–536.

Lobo-Guerrero, S., and Vallejo, L. E., (2006). “Discrete element method analysis of railtrack ballast degradation during cyclic loading”. J. Granular Matter 8: 195–204. © Springer-Verlag 2006.

Olowokere, D. O. (1975). “Strength and deformation of railway ballast subject to triaxial loading”. M.S. Thesis, Dept of Civil Engineering, Queen’s University, Kingston, Ontario, Canada.

Potyondy, D.O., and Cundall, P. A. (2004). “A bonded-particle model for rock”. Int. Journal of Rock Mechanics and Mining Sciences 41, 1329–1364.

Potyondy, D.O. (2015). “The Bonded-Particle Model as a tool for rock mechanics research and application: Current trends and future directions”. Geosystem Engineering, 18(1), 1-28.

Selig, E. T., and Waters, J. M. (1994). “Track geotechnology and substructure management”. Thomas Telford.

Shenton, M. J., (1975). “Deformation of railway ballast under repeated loading conditions”. Railroad Track Mechanics and Technology (Kerred.), Princeton University, 387–404.

Suiker, A. S., Selig, E. T., and Raymond, F. (2005). “Static and cyclic triaxial testing of ballast and subballast”. J. Geotech. Geoenviron. Eng., 131(6): 771-782.

Sun, Q. D., Indraratna, B., and Nimbalkar, S. (2015). “Deformation and degradation mechanisms of railway ballast under high frequency cyclic loading”. J. Geotech. Geoenv. Eng., 10.1061/(ASCE)GT.1943-5606.0001375, 04015056.

Yang, B., Jiao, Y. and Lei, S. (2006). “A study on the effects of microparameters on macroproperties for specimens created by bonded particles”. Engineering Comput. Int. J. Computer Aided Engineering Software. 23, 607-631.

CHAPTER 3: APPROXIMATING POLYHEDRAL BALLAST SHAPES USING AGGLOMERATES OF SPHERES TO STUDY BALLAST LAYER RESPONSE UNDER TRAIN LOADING[2]

Abstract

Particle shape and minerology have been found to have a strong impact on railroad ballast response under train loading. In this research effort, real ballast shapes were digitized using an inexpensive imaging tool, and agglomerates of spheres were used to regenerate those complex shapes. Particle crushing tests were carried out in the laboratory, and discrete element models simulating the crushing test were calibrated based on the laboratory test results. Model parameters established through this calibration process were subsequently used to study the permanent deformation response of ballast layers comprising complex-shaped breakable ballast particles under repeated loading. The effect of particle shape was studied by comparing the permanent deformation behavior for ballast layers comprising simplified ellipsoid particles to those comprising the complex-shaped particles simulated using agglomerates of spheres.

Keywords: Discrete Element Method; Railroad Ballast; Permanent Deformation; Particle Crushing Test

[2] This chapter includes results reported in the following publication. Contribution of the coauthor is sincerely acknowledged:

Dahal, B., and Mishra, D. (2019). "Simulating Polyhedral Ballasts Shapes to Study Ballast Layer Response under Train Loading". Journal of Computer and Geotechnics (in preparation).

Introduction

As a part of the railroad track substructure, the ballast layer performs various functions like resisting the vertical, longitudinal and transverse forces from trains; distributing the high stresses to protect the underlying track layers; absorbing the shock from dynamic loads from moving trains, and facilitating the free drainage conditions (Nimbalkar and Indraratna, 2015). As the ballast layer ages, it is progressively fouled with materials that are finer than the initial ballast aggregates (Qian et al., 2014). The main cause of ballast fouling is attributed to ballast degradation and breakdown of the uniformly-graded ballast aggregates under repeated train loading (Selig et al., 1988; Selig et al., 1992). It has been reported that approximately 76% of the ballast layer fouling occurs due to ballast breakage (Selig and Waters, 1994). Particle breakage significantly influences the shear strength and deformation behaviors of railroad ballast layers (Anderson and Key, 2000; Indraratna et al., 1998), resulting in unacceptable differential settlement of track and pumping of underlying soft subgrade soils which eventually necessitate frequent costly track maintenance (Indraratna and Nimbalkar, 2011). Accordingly, to study the influence of particle breakage on the strength and deformation characteristics of granular soils, many experimental (Shenton, 1975; Indraratna et al., 1998; Lackenby et al., 2007; Aursudkij et al., 2009; Indraratna et al., 2010a) and numerical-discrete element (DE) (Lim and McDowell, 2005; Lobo-Guerrero and Vallejo, 2006; Lu and McDowell, 2010) studies have been conducted. Numerical studies have been frequently used for the ballast breakage studies as they give a complete picture of where the degradation starts, how it evolves, and how it affects the permanent deformation of railroad tracks (Lobo-Guerrero and Vallejo, 2006).

Most three-dimensional DE codes use spheres to represent particle shapes due to their ease in the detection of inter-particle contact and force calculation. Models to describe the physics of contacts between spheres with walls, and with each other are relatively well-known (Di Maio and Renzo, 2004; Kruggel-Emden et al., 2007). Spheres can be used to approximate the qualitative behavior of the granular materials, but cannot give the information on the quantitative measures and therefore show deviant mechanical behavior than the actual material in consideration (Latham and Munjiza, 2004; Kruggel-Emden et al., 2009; Jean-Francois and McDowell, 2010). Particle shape, size and minerology have been found to have significant impacts on the mechanical behavior of the granular media (Azéma, 2013; Höhner et al., 2013). However, representation of the particle shape has been one of the main challenges of DE simulations (Markauskas et al., 2010). There are DEM tools such as like BLOKS3D that can simulate actual interaction between the polyhedral shapes (Zhao et al., 2006) but are not able to simulate breakages. Hence, using PFC3D this research study uses the concept of agglomerates where spheres are bonded together to represent the complex and irregular polyhedral particle shapes as they can make the contact detection and force calculation easy. Similar approaches have been used by McDowell and Harireche (2002), Thornton and Liu (2004), and Alshibli and Cil (2014) to model the particle breakage. It should be noted that in the remainder of this chapter, polyhedral and ellipsoid shapes were actually approximated by using agglomerates of bonded spheres. To understand the significance of ballast breakage considerations on permanent deformation behavior of railroad ballast layer under repeated loading, the authors initially conducted a study using simple ellipsoid shapes as representative ballast shapes and reported the findings in an earlier manuscript Dahal et al. (2018). Note that findings from this earlier

manuscript were presented in Chapter 2 of this thesis. However, since the ballast particles in Dahal et al. (2018) were simulated as ellipsoids, the results were arguably different from real-world scenarios where the ballasts are polyhedral in nature. Besides, the bond strength values (primarily governing the particle breakage; reported on Chapter 2 of this thesis) assigned to the ballast agglomerates were modified from the values obtained from the literature (Indraratna et al., 2010a). Accordingly, subsequent research tasks focused on improving the previous model, to simulate realistic ballast shapes. Findings from this improvement effort have been reported in this chapter.

Research Objective

The ultimate objective of this research effort was to study the importance of considering realistic particle shapes during discrete element modeling while studying the permanent deformation and breakage behavior of railroad ballast under repeated loading. To achieve this objective, one of the tasks involved conducting laboratory tests to quantify the crushing strengths for actual ballast particles, and calibrating DE models of the crushing strength test to establish relevant model parameters to be used in subsequent tasks. The final objective of this paper was to compare the results obtained for complex-shaped ballast particles (simulated using the agglomerates of spheres) to those obtained for simplified ellipsoid shapes; this would help identify the importance of considering realistic particle shapes during discrete element modeling.

Acquisition of Real Ballast Shapes

Several researchers have used expensive and complex image analysis approaches to create polyhedral particles for use in DE simulations (Paixão et al., 2001; Le Pen et al., 2013; Qian et al., 2013; Sun et al., 2014). However, such expensive imaging equipment to

obtain the scanned 3D image of the ballast shapes are not readily accessible. In such instances, exploration of alternative inexpensive alternatives to digitize realistic ballast particle shapes becomes imperative. With the advent of modern smartphones, it has become increasingly easier to capture high-resolution images that can be easily digitized. This research effort utilized such an approach to digitize actual ballast particle shapes, that were subsequently imported into the DE model. Three different ballast shapes were selected to demonstrate this approach. To capture the images, each ballast was placed on a flat surface such that the flattest part of the particle rested on the platform. More than twenty (20) sequential images of the ballast particles were taken by rotating the particles from 0º-360º on a horizontal plane, and the images were then imported into the Autodesk Recap Software (Autodesk, 2018). The flat surface was closed using a built-in feature of the software, and was finally exported in. stl format to be used in PFC3D (DE software). Figure 3-1 (a,b,c) and (d,e,f) show the chosen ballast shapes and exported images of ballasts from the software for Ballast 1 (B1), Ballast 2 (B2) and Ballast 3 (B3) respectively. These shapes were approximated within PFC 3D using the agglomerates of spheres to be used in the subsequent simulations.

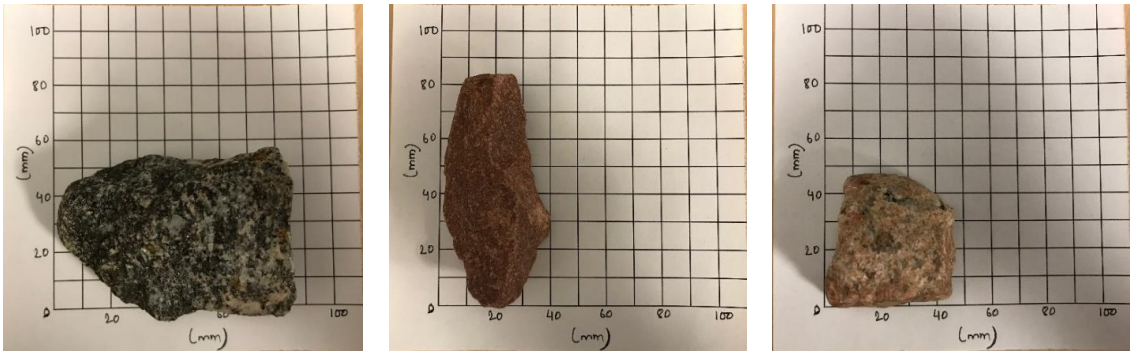

(a) (b) (c)

(d) (e) (f)

Figure 3-1: Images of (a) B1, (b) B2, and (c) B3 ballast particles captured using a smartphone; Same images have been digitized using Autodesk Recap software (d, e, f, respectively)

Laboratory Specific Gravity Test

The specific gravity test was conducted to obtain the density of ballast particles to be used in the DE model. Specific gravity of the selected ballasts was calculated using the following procedure. The test apparatus was set up and the temperature of water was set to 25°C. Each ballast particle was taken separately and was weighed to calculate its dry weight (W_1). The particle was then put in water and weighed (W_2). Finally, the particle was removed from water, surface dried with a towel by rolling inside a towel for approximately 5 seconds, and weighed to obtain the surface dry weight (W_3). The specific unit weight or specific gravity was calculated using the equation below.

$$\text{Specific Gravity} = \frac{W_1}{W_3 - W_2}$$

The specific gravity values for B1, B2 and B3 were obtained to be 2741 kg/m^3, 2555 kg/m^3, 2534 kg/m^3 respectively.

Single Particle Crushing Test

Several different factors such as angularity, uniformity of gradation, lower particle strength, coarseness, stress level and anisotropy stimulate the crushing of railroad ballast (Bohac et al., 2001). The most important of all these factors is the crushing strength of ballast. Appropriate particle crushing strength values can be established by performing the Single Particle Crushing Test (SPCT) in the laboratory. The SPCT is an indirect tensile test that is conducted by compressing individual particles between two flat platens to induce tensile stresses in the particles (Lim, 2004). A typical result of this crushing test is a plot of force against deformation. The maximum peak load is the point at which major fracture occurs along the loading direction whereby the particle splits into two or more pieces.

Laboratory Crushing Test

A Universal Testing Machine (UTM) was used to perform the laboratory tests on the three ballast particles. Since the shapes of the particles were irregular and coarse, they were aligned on the bottom platen in such a way that each particle rested with its flattest portion on bottom platen of the machine. Figure 3-2-a and Figure 3-2-b show the test set up for SPCT and B1 particle in the test setup for crushing, respectively. Load was then applied by moving the top platen downwards at 1.9 mm/sec. Force and displacement data were continuously collected throughout the test.

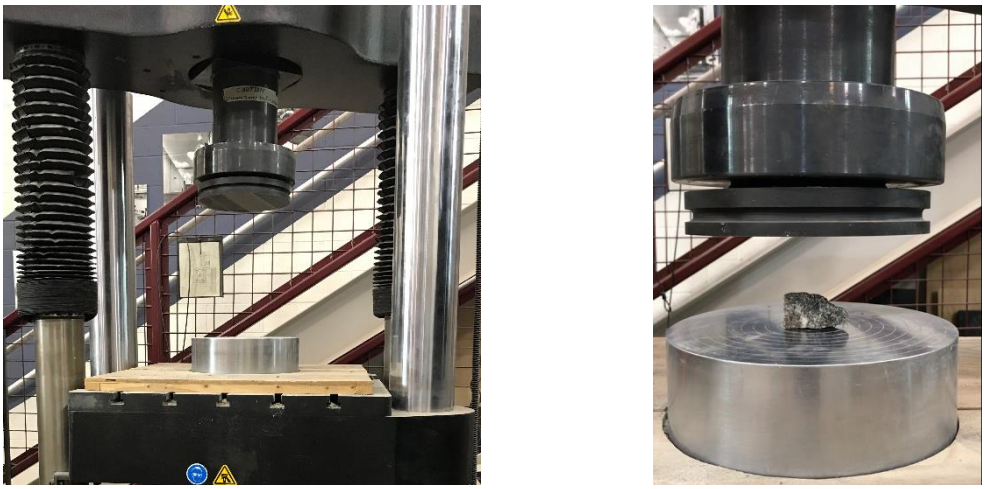

(a) (b)

Figure 3-2: (a) Test setup for SPCT (b) Ballast Particle B1 in Test Setup

Figure 3-3 shows the force-displacement plot obtained for the particle B1, B2 and B3. From the figure, it can be seen that the load-displacement plot went through several undulations owing shifting and reorientation of the ballast particle during the loading process. These displacements were not included in the final force-displacement calculations. Similar results were obtained for ballast particles B2 and B3.

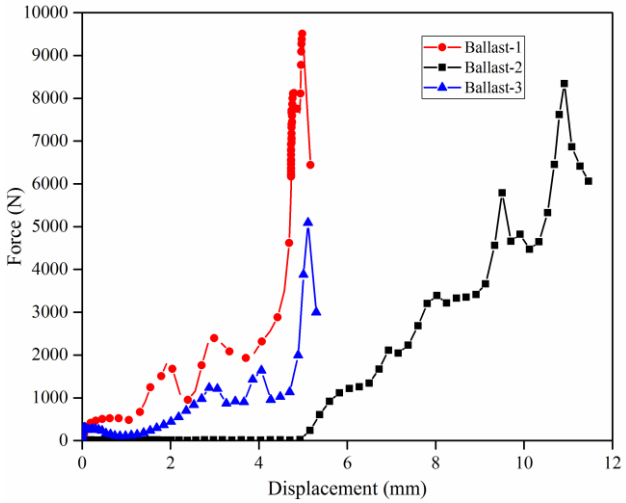

Figure 3-3: Lab obtained force vs displacement data during SPCT on Ballast Particles B1, B2 and B3

Figure 3-4 shows photographs of the ballast particles after they have been crushed in the laboratory. After the crushing strength for each ballast particle was established, the next

step involved DE modeling and calibration of this crushing test.

(a) (b) (c)

Figure 3-4: Photographs showing the ballast particles after laboratory crushing tests: (a) B1 (b) B2 (c) B3

Discrete Element Simulation of the Particle Crushing Test

The material modeling support package of PFC was used to simulate the Single Particle Crushing Test (SPCT) of individual ballast particles. This support package can be used to create an assembly of packed particles under a specified material pressure and porosity, and assign the contact model of one's choice, like the linear contact model, bonded particle model, etc. On these packed assemblies, different tests such as the tension test, compression test and diametral compression test can be simulated. Detailed information about the material modeling support package can be found in the Itasca technical memorandum by Potyondy (2018). For simulating the SPCT on irregular ballasts shapes, the material modeling support package could not be used directly. Accordingly, some modifications were implemented, and new algorithms were developed to ensure the simulations accurately represented the particles tested in the laboratory.

Creation of Irregular Ballast Shapes

As already mentioned, individual particles in PFC3D are represented as spheres. Therefore, to model non-spherical particles, special care needs to be taken to combine spheres of different sizes in certain fashions so that the resulting "agglomerate" represents

the irregular shape being targeted. Once the three different ballast particles were digitized from the photographs, and their corresponding .stl files were imported into PFC3D, the next step involved recreating these particle shapes using agglomerates of spheres. This was accomplished through the following steps: First, cuboid boxes of dimensions larger than corresponding ballast particles were created, and filled with spheres of diameter 5-6 mm, and compacted to achieve a porosity value of 20% and a material pressure of 150kPa. Note that to check whether the packing pressure affects the ultimate strength of the specimen, the pressure was reduced from 150 kPa to 5 kPa; No change in the crushing strength was observed. Once the packed material was created, the spheres were bonded with linear parallel bonds with certain bond strength and modulus values. The detailed description of the linear parallel bond can be found elsewhere (Potyondy and Cundall, 2004; Potyondy, 2015). The elastic modulus of the spheres was chosen such that the stiffness of the spheres matched the stiffness of respective ballasts. The moduli and ratios of normal to shear stiffness values for spheres as well as cement (bond) of linear parallel bond were set equal to reduce the number of free parameters (Potyondy and Cundall, 2004; Potyondy, 2015). The radius multiplier term which refers to the radius of the parallel bond such that the bond radius equals the radius multiplier times the radius of the smaller sphere in contact was set to 1. Once the packed assembly was created, the geometry of the corresponding ballasts (see Figure 3-1) was imported into the model. An algorithm was developed to detect all spheres that have centroids within the geometry of corresponding shape being generated. Figure 3-5 represents cluster of bonded spheres that are within the geometry of corresponding particle being generated. This cluster of bonded spheres now represented

the irregular ballast shapes B1, B2 and B3 which were composed of 650, 216 and 254 individual spheres, respectively.

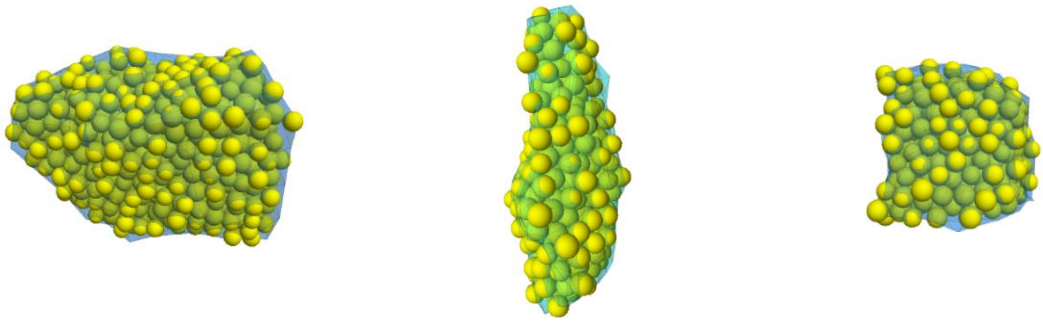

(a) (b) (c)

Figure 3-5: Cluster of bonded spheres to match the geometries of corresponding ballast particles (a) B1 (b) B2 (c) B3

Simulating the Diametral Compression (DC) Test

To subject the individual ballast particles to diametral compression test, the top and bottom walls or platens were created ensuring that they were placed exactly at the top and bottom points of the representative particles. Each of the ballast particles were oriented such that they resembled their orientation in the lab test. Tilting of the loading platens as well as that of the ballast particle were not allowed during the simulated crushing tests. The system was brought to equilibrium, displacements of the spheres were set to zero, and the loading was applied by moving the top and bottom walls at a rate of 0.2 mm/sec. The frictionless top and bottom plates were moved towards the bonded assembly representation of ballasts to simulate the crushing. Microstructural monitoring to visualize the fragments caused during the test was done whereby small red discs were created upon bond breakage at the breakage points. The test stopped when the load carrying ability of the ballast was compromised, and the axial force magnitude fell below a specified fraction of its peak value. The axial force was taken as the average force of the opposing top and bottom walls. The axial strain was based on the change of distance between the opposing walls. Figure

3-6-(a, d, g), Figure 3-6-(b, e, h), Figure 3-6-(c, f, i) represent the PFC-generated irregular ballast particles, DC test setups for the individual particles, and the broken ballast particles under peak loading, respectively.

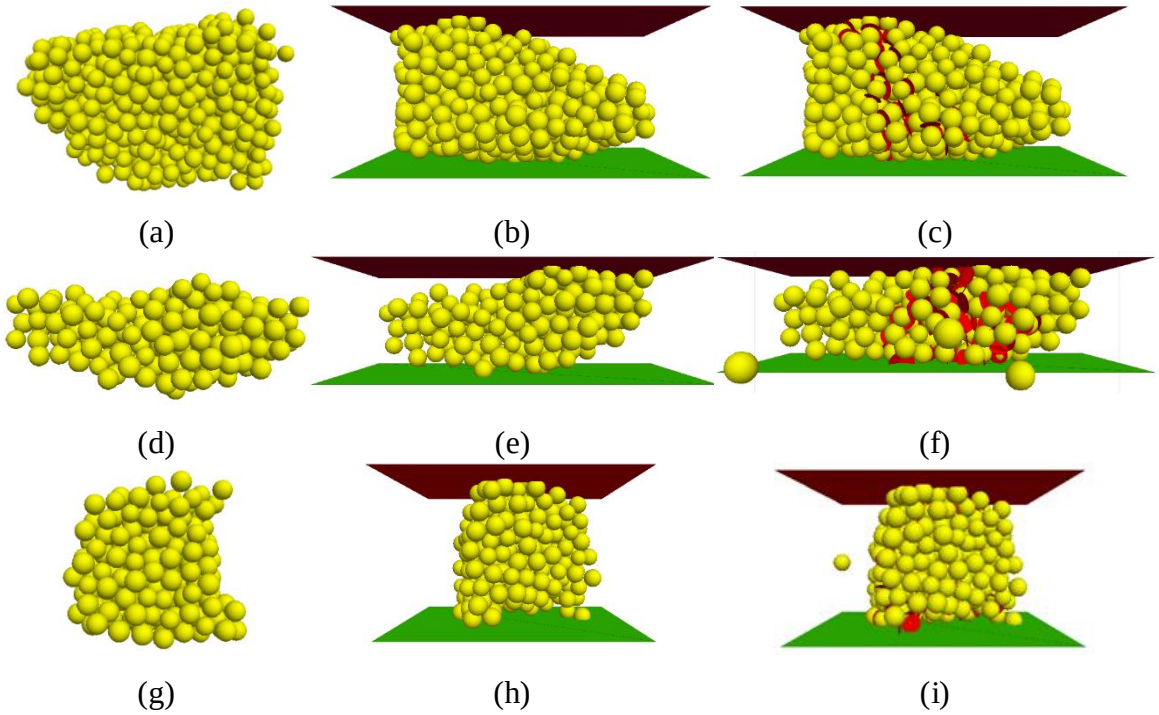

Figure 3-6: Representative irregular ballast shapes (a, d, g); DC test set-up with ballasts (b, e, h); Broken ballasts at peak load (c, f, i) for B1, B2 and B3 respectively

Table 3-1 lists the important parameters used for calibration of DC test. Table 3-2 lists the peak force and displacement values from the laboratory and the DC crushing test for the ballast particles. Even though the peak force and displacement values did not match exactly, the calibration was considered complete, as the primary intention of this research effort was to get representative ballast calibrated strength model parameters which could be used to study the effect of real polyhedral ballast layer response on ballast breakage and PD.

Table 3-1: Important Parameters used for DC Test Calibration

Name	PFC Parameter	Description	Value
Material Parameters	cm_Dlo	Lower Diameter (mm)	5
	cm_Dup	Upper Diameter (mm)	6
	cm_densityVal	Density (kg/m^3)	2741 (B1)
			2555 (B2)
			2534 (B3)
	cm_localDamp	Damping factor	0.7
	pk_Pm	Material Pressure (kPa)	150
	pk_nc	Cloud Porosity	0.2
Vessel Parameters	mv_emod	Effective Modulus (GPa)	3
Compression Test	dc_eRate	Strain Rate (mm/sec)	0.2
Parallel-Bonded Material Group	pbm_emod	Bond Effective Modulus (GPa)	1.7 (B1)
			0.4 (B2)
			0.4 (B3)
	pbm_krat	Normal to Shear Stiffness	2.0
	pbm_fric	Friction Coefficient	0.5
	pbm_ten_m	Tensile Strength (MPa)	4.5 (B1)
			4.0 (B2)
			3.0 (B3)
	pbm_coh_m	Cohesion Strength (MPa)	19 (B1)
			18 (B2)
			10 (B3)
	pbm_rmul	Radius Multiplier	1
	pbm_fa	Friction Angle	0
	pbm_igap	Installation Gap	0
Linear Material Group	lnm_emod	Effective Modulus (GPa)	1.7 (B1)
			0.4 (B2)
			0.4 (B3)
	lnm_krat	Normal to Shear Stiffness	2.0
	lnm_fric	Friction Coefficient	0.5

Table 3-2: Final Calibrated Results for Single Particle Crushing Test

S.N.	Ballast	Lab Test		Diametral Compression Test	
		Peak Force	Displacement	Peak Force	Displacement
1	Ballast-1	9510	1.27	9800	1.28
2	Ballast-2	8345	5.98	8600	6
3	Ballast-3	5093	4.13	5500	4.5

Cyclic Loading of Ballast Layer Comprising Breakable Complex-Shaped Particles

Specimen Preparation

A novel approach was used to create the ballast layer in this simulation. First, a specimen box of size 600 mm x 600 mm x 500 mm was created using PFC3D. A total of 2400 ballast particles were distributed in the specimen box using the particle size distribution shown in Figure 3-7-a. 600 ballast particles were selected from each size distribution range (varying from 15-50 mm) as shown in the inset table of Figure 3-7-a. The ballast particles were composed of equal number of particles conforming to the three different shapes: B1, B2, and B3. The ballast particle templates used in the simulation are shown in Figure 3-7-b. Each of the ballast particles B1, B2 and B3 comprises 7, 7 and 6 spheres, respectively. Note that each particle shape was represented by combining smaller number of spheres (7, 7, and 6, respectively) as the resulting reduction in computational times was necessary to complete all research tasks in time. For particles represented by agglomerates of larger number of spheres, the computational time requirements were unreasonably high (the simulation did not finish after running continuously for 75 days on a desktop computer with high processing power).

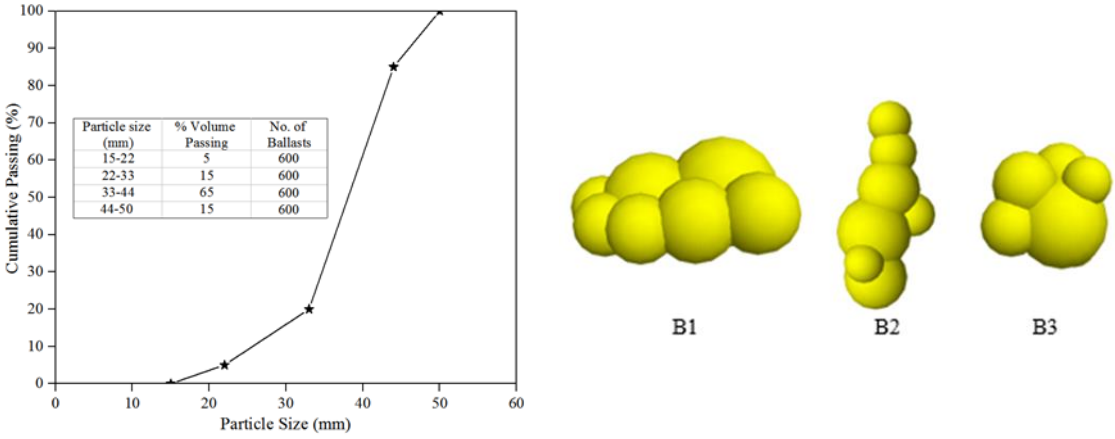

(a) (b)

Figure 3-7: (a) Particle size distribution used in the simulation; (b) Ballast templates used

Once generated, the ballast particles were allowed to settle under gravity. Under gravity, the thickness of the ballast layer became 250 mm. After this step, material pressure of 20 kPa was applied to the specimen by moving the surrounding walls via a servo mechanism to account for the confinement provided by the crossties, shoulder ballast, and crib ballasts. Note that researchers in the past have reported typical confining stress values in the range of 10-60 kPa (Indraratna, 2010b). Figure 3-8-a shows the packed ballast assembly after this stage represented in the form of spheres of ballast templates shown in Figure 3-7-b. Figure 3-8-b shows the packed assembly represented in the form of geometry of the corresponding particles in the simulation. All the model parameters used in the simulation have been listed in Table 3-3.

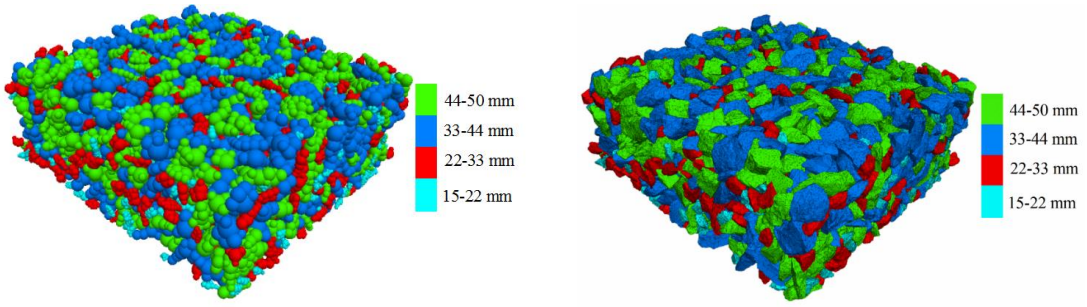

(a) (b)

Figure 3-8: Initial packed ballast assembly represented by (a) Agglomerates of spheres; and (b) Exact geometry of the particles imported

Table 3-3: Parameters used in the Simulation

Model Parameters	Values
Specimen Size	Length = 600 mm Width = 600 mm Height = 500 mm
Particle Density	2610 kg/m^3
Damping Ratio	0.7
Wall Effective Modulus	3.0 GPa
Friction Coefficient	0.6
Poisson's Ratio	0.2
Ballast Effective Modulus	0.833 GPa

The value of effective modulus used in the simulation was taken as the average of the modulus values for the three ballast particles tested in the laboratory. The friction coefficient between ballast-ballast interaction was taken as 0.6 (tan 31º) after Kwan (2006). The ballast layer was then applied with the mean stress of cyclic loading of 232 kPa via top wall of the specimen box.

Contact Model for Ballast-Ballast Interaction

Most of the researches conducted on the DE modeling of railroad ballast use the linear-elastic contact model to represent the ballast-ballast contacts. However, the linear-elastic approach can only give a crude estimate of the ballast layer response. The behavior of ballast under loading has been established to be non-linear (Lekarp et al., 2000). For this reason, in this research study, the ballast-ballast contact was modeled using a contact model

recently introduced by Itasca; the Hill Contact Model (Potyondy, 2016). This contact model provides the behavior of an infinitesimal, nonlinear elastic (no tension) and frictional interface that carries a compressive surface interaction force and may carry a tensile moisture force. The surface interaction force model is based on the Hertz-Mindlin contact theory along with a damping mechanism and Coulomb sliding friction (Tsuji et al., 1992). The surface interaction force consists of Hertzian and dashpot components with Hertz-Mindlin springs providing the nonlinear force-displacement response. The Hill Contact Model simulates the contact behavior between two locally elastic spheres that may have a liquid bridge and the material behaves like an unsaturated granular material. The liquid bridge is present if the moisture state is wet, and absent if the moisture state is dry. Detailed information on the Hill Contact Model can be found in the Itasca Technical Memorandum (Potyondy, 2016). In this simulation, the liquid bridge was not modeled, and hence the ballast-ballast contact model acted as a non-linear contact model; this can be said to be a better representation of the nature of interaction at ballast-ballast contacts compared to linear-elastic assumptions. For the ballast-specimen box interaction, the linear contact behavior was assumed.

Simulation of Breakable Ballast Particles

Once the mean stress of cyclic loading of 232 kPa was applied to the system, the non-breakable ballasts were freed, and replaced with clusters of spheres with same radii at the same positions, and bonded together using linear-parallel bonds. For simplicity, the average of bond strengths and stiffness values obtained from the DC calibration tests were used in this simulation. Breakage of the bonds within the spheres in each cluster was considered as particle breakage. Upon breakage of the linear parallel bonds under the load,

the default contact of Hill contact model was applied to each new ballast-ballast contact. Table 3-4 shows the bond strength parameter values for the linear parallel bonds used in this study.

Table 3-4: Bond Strength Parameters for Linear Parallel Bonds

Parallel Bond Parameters	Values
Parallel Bond Normal Stiffness ($\overline{k_n}$)	1.48×10^{11} N/m^3
Parallel Bond Shear Stiffness ($\overline{k_s}$)	7.58×10^{10} N/m^3
Parallel Bond Normal Strength (σ)	3.83×10^{6} N/m^2
Parallel Bond Shear Strength (τ)	1.57×10^{7} N/m^2

After this step, cyclic loading was applied to the ballast layer via the top wall of the specimen box. Figure 3-9 shows the typical cyclic loading curve used in the simulation. Detailed description of the cyclic load applied in this simulation can be found in Dahal et al. (2018), and have been described in Chapter 2 of this thesis.

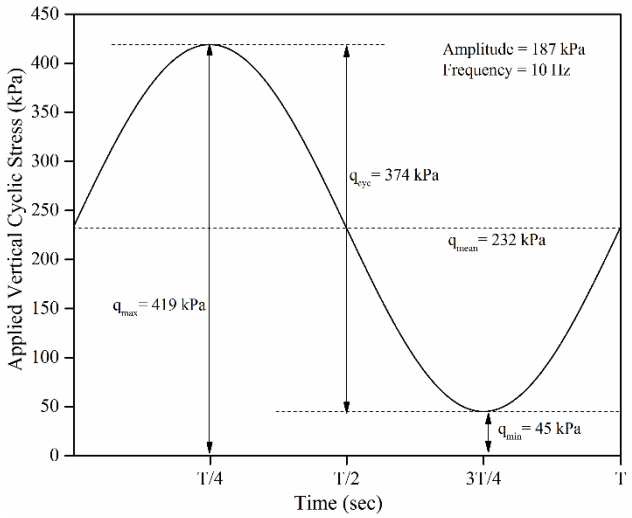

Figure 3-9: Typical cyclic loading curve used in the simulation

Results and Discussion

The ballast layer was subjected to 50 load cycles, and the stress-strain responses were recorded. Strain was calculated in terms of percentage and was taken as the distance between top and bottom wall after loading divided by the initial distance between the walls.

Stress was taken as the ratio of the load experienced by the top wall to the area of the top wall.

Study of Ballast Permanent Deformation

Figure 3-10-a shows the evolution of vertical strain with the number of load cycles. As seen from the figure, there was an initial bulging of approximately 8%. This can be attributed to the overlap between the spheres forming the ballasts shapes. Once there is a breakage in the specimen, the forces associated with the ballast particle overlap result in the instant bulging of the ballast layer. After the energy has been released, there is sudden increase in the vertical axial strain with the initial load cycles. This sudden increase in the permanent deformation accumulation can be attributed to the ballast breakage which is the highest during the initial load cycle. After the initial cycle, the axial strain is found to increase in a steady manner and towards the end of 50 load cycles, the cyclic part of the axial strain is constant, and the permanent deformation accumulation is found to have stabilized. This can be explained by the fact that after the initial breakage, the broken ballast particles rearrange themselves in the void spaces, thereby densifying the ballast. The total vertical permanent strain accumulation was calculated as 16.63 mm (7.66%) after 50 load cycles.

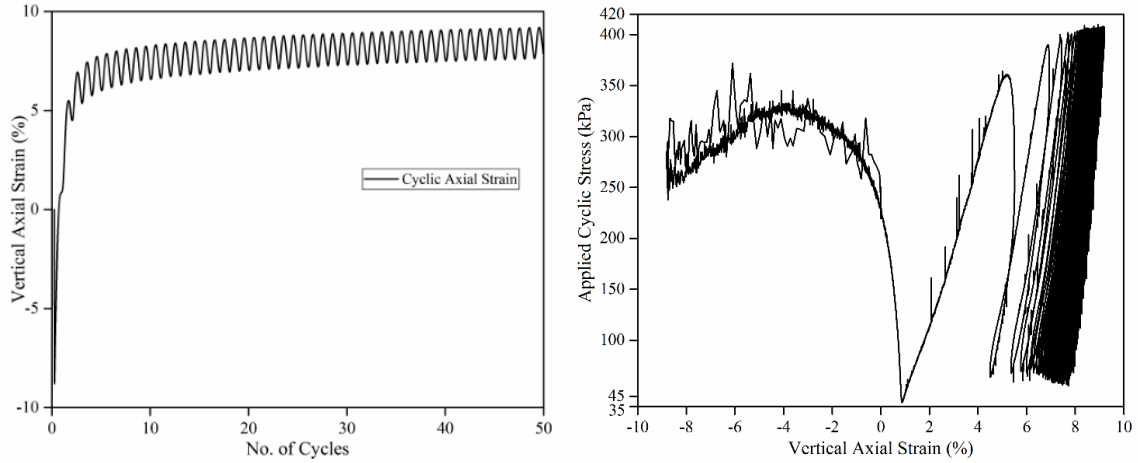

(a) (b)

Figure 3-10: (a) Vertical axial strain vs No. of cycles (b) Applied cyclic stress vs Vertical axial strain

Figure 3-10-b shows the applied cyclic stress plotted against the vertical strain for 50 load cycles. Initially, the axial strain is negative in the figure which corresponds to bulging of the specimen. After the bulging is over, the axial strain accumulation after first few load cycles is significantly higher than under successive load cycles (about 6% permanent deformation accumulation). In this plot, the spikes in the stress-strain response during the first few load cycles can be attributed to particle breakages. However, once the initial load cycles have been completed, the ballast stress-strain response is more or less elastic showing a near-complete hysteretic behavior towards the end of 50 load cycles. This demonstrates the resilient behavior of ballast layer once it is subjected to large number of load cycles. Similar trends were reported by Indraratna et al. (2010a).

Study of Ballast Breakage

Figure 3-11-a and Figure 3-11-b show plan views of the ballast box before and after application of the cyclic loading, respectively. The ballast particles can be seen to have undergone significant breakage, and the initial and final ballasts orientation cannot be

distinguished due to the rearrangement of the broken ballast particles. For example, the rectangular portion of Figure 3-11-a and Figure 3-11-b have been enlarged in Figure 3-11-c. The red ballast particles in the rectangular portion in Figure 3-11-c have completely broken down after cyclic load application. Similar is the case for the green, cyan, as well as blue ballast particles. These broken ballast particles eventually move to the void space in the assembly, and result in permanent deformation accumulation. Therefore, particle breakage and subsequent rearrangement of the broken particles act as governing factors for cyclic densification of the assembly.

To quantify the number of breakages in terms of bond breakage in the cluster of spheres forming ballast particles, the number of linear parallel bonds before and after the cyclic load application were tracked. The number of linear parallel bonds before and after cyclic load application were 23200 and 937, respectively; a total of 22263 bonds were broken under cyclic loading. Most of these bonds were found to be broken during the initial load cycles leading to sudden increase in permanent deformation accumulation under the initial load cycles. Once the bond breakage ceased, no significant increase in permanent deformation accumulation was observed. This clearly highlights the fact that particle breakage is the major source of permanent deformation accumulation in ballast layers. Figure 3-12-a and Figure 3-12-b show the number of linear parallel bonds before and after cyclic load application, respectively.

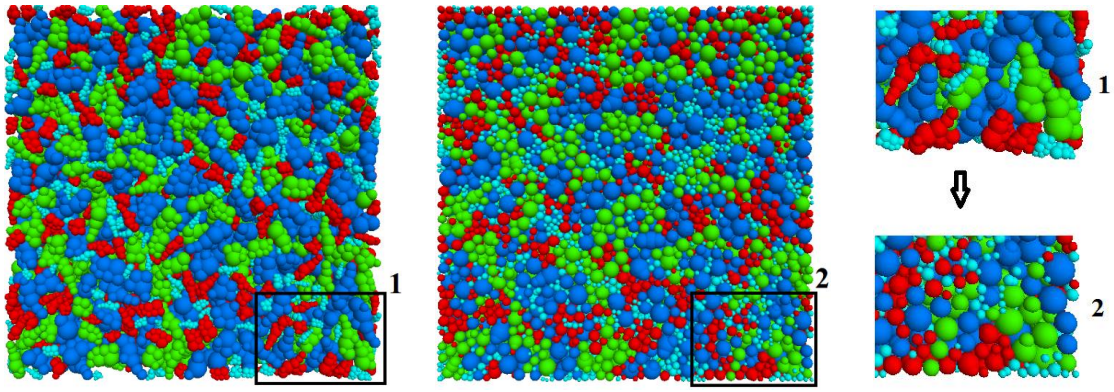

(a) (b) (c)

Figure 3-11: Change in ballasts orientation (a) Before cyclic loading (b) After cyclic loading (c) Enlarged rectangular portion of (a) and (b) respectively

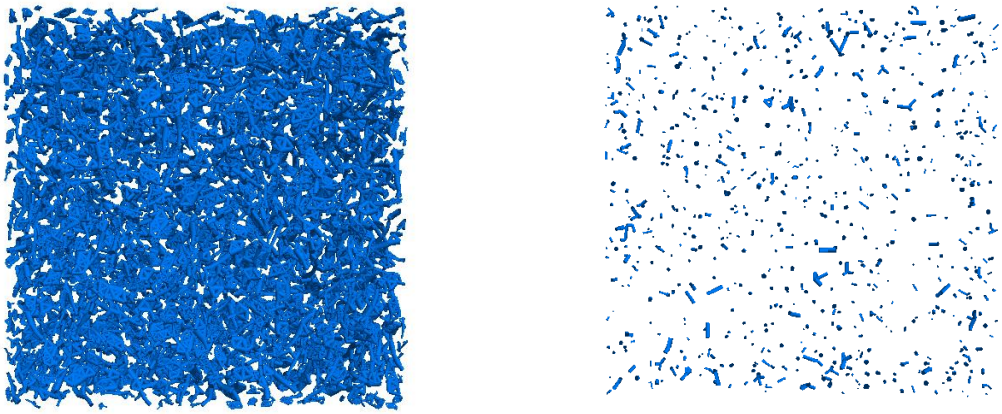

(a) (b)

Figure 3-12: Linear Parallel Bonds in the Ballast Assembly (a) Before; and (b) After Cyclic Load Application

The Contact Force (CF) chains between ballast particles before and after cyclic loading have been plotted in Figure 3-13-a and Figure 3-13-b. As seen from these figures, the contact force chains are more uniform and widely distributed in the after-cyclic loading configuration, indicating good contacts between the ballast particles. This is because under loading the ballast particles undergo breakage resulting in the rearrangement of broken ballast particles in the void spaces present in the assembly. Note that the contact force chains in the plots are scaled by force, and the thickness of the lines correspond to the force magnitudes. Observing the contact force distribution after cyclic loading, it can be

concluded that particle breakage plays a critical role in controlling the development of CF chains and governing the load distribution pattern in granular media under cyclic loading.

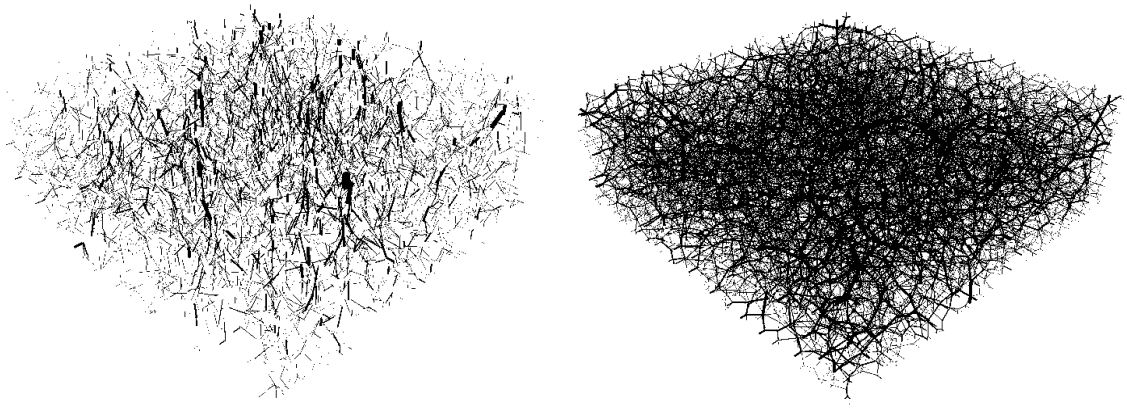

(a) (b)

Figure 3-13: (a) Contact force chains in the Ballast Layer (a) Before cyclic loading and (b) After cyclic loading

Importance of Accurate Representation of Ballast Particle Shape during DEM Simulation

To assess the importance of accurate representation of ballast particle shapes during DEM simulations, the exact same simulations steps described above, were repeated for ellipsoid ballast particles. Figure 3-14-a and Figure 3-14-b show the plots for permanent strain accumulation with number of load cycles and change in particle size distribution before and after cyclic load for the complex-shaped as well as ellipsoid ballast particles. Note that in the figures, the complex-shaped ballast particles (e.g. B1, B2, and B3) have been referred to as polyhedral particles. It is important to note that this research effort did not use actual polyhedral particles, rather, used agglomerates of spheres to represent complex-shaped particles.

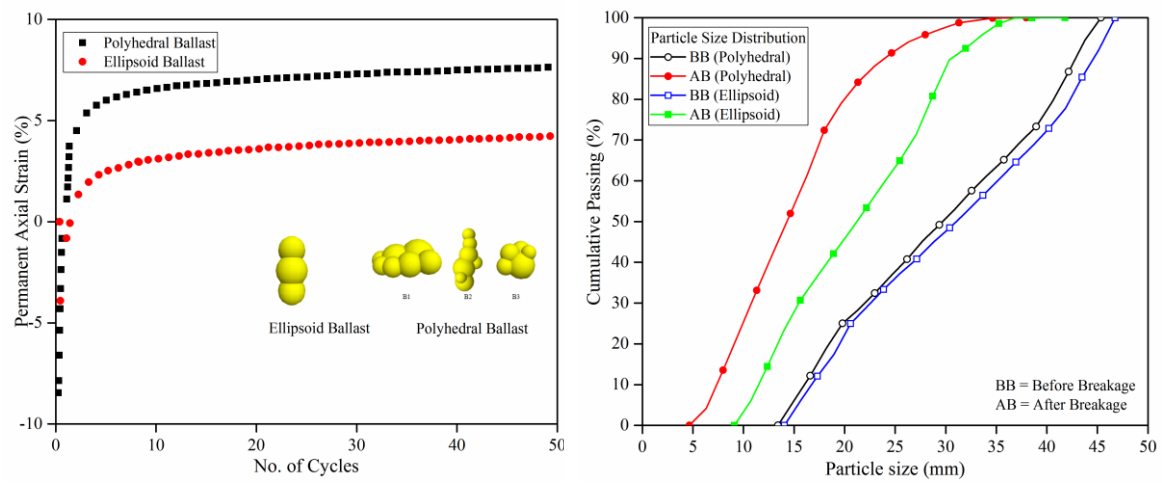

(a) (b)

Figure 3-14: (a) Permanent strain or PD accumulation vs No. of cycles for polyhedral and ellipsoid ballast layers (b) Change in particle size distribution before and after cyclic load application for ballast layers comprising polyhedral and ellipsoid particles

The initial bulging of the specimen of polyhedral ballasts was 8.80% while the same for the ellipsoid ballasts was 3.93%. On comparing this initial bulging, polyhedral ballasts layer bulged approximately 124% more than the ellipsoid ballast layer. The accumulated permanent deformation at the end of 50 load cycles was 7.63% for polyhedral ballast layer and 4.23% for ellipsoid ballast layer. The accumulated permanent deformation for polyhedral ballast layer was approximately 80% more than the ellipsoid ballast layer. Moreover, comparing the shift in particle size distribution before and after the cyclic loading for the two different particles shapes, it can be seen that the complex-shaped particles undergo significantly higher degree of breakage compared to ellipsoid particles. On comparing the area of particle breakage (area between the particle size distribution curves before and after cyclic loading), the areas were calculated to be 956.5 mm^2 and 1462.38 mm^2 for ellipsoid and polyhedral ballast, respectively. This shows that complex-shaped ballast particles underwent significantly higher breakage (about 53% more) compared to the ellipsoid particles under cyclic loading. From these results it can be

concluded that accurate representation of ballast particles shapes is of utmost importance during DEM simulations to accurately capture particle breakage and permanent strain accumulation trends under cyclic train loading. At this point, it should be noted that differences in particle shape did not have a significant effect in the total permanent deformation accumulation for non-breakable particles, as reported in Chapter 2 of this thesis (refer to Figure 2-6). However, when particle breakage is taken into consideration, particle shape plays a significant role in governing the total permanent deformation accumulation under loading.

Summary and Conclusion

1. A novel approach was used to generate and model complex-shaped ballast particles for DEM simulations. Single Particle Crushing Tests were carried out in the laboratory, and DE models simulating these tests were calibrated to establish relevant model parameters.
2. Using the calibrated model parameters, the permanent deformation and breakage response of ballast layers were studied under repeated loading.
3. Based on the simulation results, it was observed that particle breakage plays a significant role in governing the overall permanent deformation accumulation in ballast layers under repeated loading.
4. A major portion of ballast breakage occurred during the initial load cycles, which also corresponded to high permanent deformation accumulations. As the breakage ceased under subsequent load cycles, the rate of permanent deformation accumulation also reduced.
5. Importance of the use of polyhedral ballast shapes was assessed by comparing the

permanent deformation and shift in particle size distribution curves for complex-shaped and ellipsoid ballast particles.

6. Significant changes in the extent in particle breakage and associated permanent deformation accumulation were when the ballast particle shapes were changed from complex-shaped (polyhedral) to ellipsoid.

Limitations and Scope for Further Research

1. The exact complex-shaped particles created and used in the crushing test simulations were not used while studying the ballast layer response under repeated loading. Using the exact same particle shapes would be ideal as the calibration parameters would then be directly validated. However, simplified shapes were used in the ballast assembly during the current study because the high number of spheres required to exactly represent the complex-shaped ballast particles led to unreasonably long computational times.
2. The complex-shaped as well as ellipsoid particles used in this research effort were approximated using the agglomerates of bonded spheres. Performing the study on ballast assemblies comprising actual polyhedral particles would facilitate better representation of real ballast behavior.
3. The next step of this research would be to calibrate or verify the ballast response obtained from this research by comparing with the full-scale cyclic plate load box tests.

References

Alshibli, K.A., and Cil, M.B. (2014). “3D evolution of sand fracture under 1D compression". Géotechnique 64 (5) (2014) 351–364.

Anderson, W.F., and Key, A.J. (2000). “Model testing of two-layer railway track ballast”. J. Geotech. and Geoenv. Eng; 126, 317–323.

Aursudkij, B., McDowell, G.R., and Collop, A.C. (2009). “Cyclic loading of railway ballast under triaxial conditions and in a railway test facility”. Granular Matter; 11(6), 391–401.

Autodesk Inc. (2018). https://www.autodesk.com/products/recap/overview

Azéma, E., Radjai, F., and Dubois, F. (2013). “Packings of irregular polyhedral particles: Strength, structure, and effects of angularity”. Physical Review E; 87(6), 062203.

Bohac, J., Feda, J., and Kuthan, B. (2001). “Modelling of grain crushing and debonding”. Proc. 15th Int. Conf. on Soil Mech. and Geotech. Eng. 2001; Vol. 1, pp. 43-46.

Dahal, B., Mahmud, S. N. M., and Mishra, D. (2018). “Simulating ballast breakage under repeated loading using the discrete element method”. Proceedings of the 2018 Joint Rail Conference, April 18-21, 2018, Pittsburgh, PA.

Di Maio, F.P., and Renzo, A.D. (2004). “Analytical solution for the problem of frictional-elastic collisions of spherical particles using the linear model”. Chemical Engineering Science; 59 (16) 3461–3475.

Höhner, D., Wirtz, S., and Scherer, V. (2013). “Experimental and numerical investigation on the influence of particle shape and shape approximation on hopper discharge using the discrete element method”. Powder Technol.; 235 614–627.

Indraratna, B., Ionescu, D., and Christie, H. (1998). “Shear behavior of railway ballast based on large-scale triaxial tests”. J. Geotech. and Geoenv. Eng; 124, 439–449.

Indraratna, B., and Nimbalkar, S. (2011). “Implications of ballast breakage on ballasted railway track based on numerical modelling”. 13th Int Conf of International Assoc for Comp. Methods and Advances in Geomechanics; p. 1085–1092.

Indraratna, B., Thakur, P.K., and Vinod, J.S. (2010a). “Experimental and numerical study of railway ballast behavior under cyclic loading”. Int. J. Geomech.; 10(4), 136–144.

Indraratna, B., Nimbalkar, S., Christie, D., Rujikiatkamjorn, C., and Vinod, J.S. (2010b). “Field assessment of the performance of a ballasted rail track with and without geosynthetics”. J. Geotech. Geoenv. Eng.

Jean-Francois, F., McDowell, G.R. (2010). “A method to model realistic particle shape and inertia in DEM”. Springer 2010.

Kruggel-Emden, H., Simsek, E., Rickelt, S., Wirtz, S., and Scherer, V. (2007). “Review and extension of normal force models for the Discrete Element Method”. Powder Technology; 171 (3) 157–173.

Kruggel-Emden, H., Wirtz, S., and Scherer, V. (2009). “Applicable contact force models for the discrete element method: the single particle perspective”. Journal of Pressure Vessel Technology; 131 (2) 024001.

Kwan, C.C.J. (2006). “Geogrid reinforcement of railway ballast”. Ph. D. Thesis; University of Nottingham.

Lackenby, J., Indraratna, B., McDowell, G., and Christie, D. (2007). “Effect of confining pressure on ballast degradation and deformation under cyclic triaxial loading”. Géotechnique; 57(6), 527–536.

Latham, J.P., and Munjiza, A. (2004). “The modelling of particle systems with real shapes”. Philosophical Transactions of the Royal Society of London, Series A: Mathematical Physical and Engineering Sciences; 362 (1822) 1953–1972.

Lekarp, F., Isacsson, U., and Dawson, A.R. (2000). “State of the art. I. Resilient response of unbound aggregates”. ASCE J. Transport Eng 2000; 126(1), 66–75.

Le Pen, L.M., Powrie, W., Zervos, A., Ahmed, S., and Aingaran, S. (2013) “Dependence of shape on particle size for a crushed rock railway ballast”. Granular Matter; 15(6), 849–861.

Lim, W.L. (2004). “Mechanics of railway ballast behavior”. Ph. D Thesis; University of Nottingham.

Lim, W.L., and McDowell, G.R. (2005). “Discrete element modelling of railway ballast”. Granular Matter; 7(1), pp. 19–29.

LoboGuerrero, S., and Vallejo, L.E. (2006). “Discrete element method analysis of railtrack ballast degradation during cyclic loading”. Granular Matter; 8(3-4), pp. 195–204.

Lu, M., and McDowell, G.R. (2010). “Discrete element modelling of railway ballast under monotonic and cyclic triaxial loading”. Geotechnique; 60(6), pp. 459–467.

Markauskas, D., Kacianauskas, R., Dziugys, A., and Navakas, R. (2010). “Investigations of adequacy of multi-sphere approximation of elliptical particles for DEM simulations”. Granular Matter; 12 (1) 107–123.

McDowell, G.R., and Harireche, O. (2002). “Discrete element modelling of yielding and normal compression of sand”. Géotechnique; 52(4), 299–304.

Nimbalkar, S., and Indraratna, B. (2015). “Implications of ballast degradation under cyclic loading”. University of Wollongong, 12th ANZ Conference on Geomechanicc.

Paixão, A., Resende, R., and Fortunato, E. (2018). “Photogrammetry for digital reconstruction of railway ballast particles – A cost-efficient method”. Const. and Bldg Mat.

Potyondy, D.O., and Cundall, P.A. (2004). “A bonded-particle model for rock”. Int. Journal of Rock Mechanics and Mining Sciences; 41(8 SPEC.ISS.), 1329–1364.

Potyondy, D.O. (2015). “The Bonded-Particle Model as a Tool for Rock Mechanics Research and Application: Current Trends and Future Directions”. Geosystem Engineering, 18(1), 1-28.

Potyondy, D. (2016). “Hill Contact Model [version 4]”. Itasca Consulting Group, Inc., Minneapolis, MN, Technical Memorandum ICG7795-L, October 12, 2016.

Potyondy, D. (2018). “Material-modeling support in PFC [fistPkg26]. Itasca Consulting Group, Inc., Minneapolis, MN, Technical Memorandum ICG7766-L, August 24, 2018.

Qian, Y., Lee, S., Tutumluer, E., Hashash, Y., Mishra, D., and Ghaboussi, J. (2013). “Simulating Ballast Shear Strength from Large-Scale Triaxial Tests”. Transportation Research Record: Journal of the Transportation Research Board; 2374, 126–135.

Qian, Y., Tutumluer, E., Hashash, Y.M.A., and Ghaboussi, J. (2014). “Effect of ballast degradation on permanent deformation behavior from large scale triaxial tests”. 2014 Joint Rail Conference, April 2-4, 2018 Colorado Springs, CO.

Selig, E.T., Collingwood, B.I., and Field, S.W. (1988). “Causes of fouling in track”. AREA Bulletin 717 1988.

Selig, E.T., Dello Russo, V., and Laine, K.J. (1992). “Sources and causes of ballast fouling”. Report No. R- 805; Association of American Railroads, Technical Center, Chicago.

Selig, E.T., and Waters, J.M. (1994). “Track geotechnology and substructure management”. Thomas Telford Publications, London.

Shenton, M.J. (1975). “Deformation of railway ballast under repeated loading conditions”. Railroad track mechanics and technology (Kerred.), Princeton University; 387–404.

Sun, Y., Indraratna, B., and Nimbalkar, S. (2014). “Three-dimensional characterisation of particle size and shape for ballast”. Géotechnique Letters; 4(3), 197–202.

Thornton, C., and Liu, L. (2004). “How do particles break?”. Powder Technol. 2004; 143(144), 110–116.

Tsuji, Y., Tanaka, T., and Ishida, T. (1992). “Lagrangian numerical simulation of plug flow of cohesionless particles in a horizontal pipe”. Powder Tech., 71(3), 239–250.

Zhao, D., Nezami, E. G., Hashash, Y. M., and Ghaboussi, J. (2006). “Three-dimensional discrete element simulation for granular materials”. Engineering Computations, 23.

CHAPTER 4: EFFECT OF GEOGRID INCLUSION ON BALLAST BREAKAGE: A NUMERICAL STUDY USING THE DISCRETE ELEMENT METHOD[3]

Abstract

Under train loading, ballast particles can undergo significant breakage resulting in overall reduction in ballast shear strength, and deterioration in the drainage properties. Placing geogrids in the ballast layer can significantly improve the mechanical response under loading, manifested through increased shear strength and improved resistance to permanent deformation. An ongoing research study at Boise State University is focusing on numerically studying the effect of geogrid reinforcement on ballast particle breakage under repeated loading. A commercially available discrete element modeling package, PFC3D® is being used for this purpose. The study makes innovative use of the Pavement Design Package, a feature built into the PFC software package. This paper presents findings on how the geogrid placement in the ballast layer affects the amount of ballast breakage and the associated permanent deformation experienced by the ballast layer. Two different geogrid types, with square as well as triangular apertures, have been studied in this modeling effort.

[3] This chapter includes results already reported in the following publication. Contribution of the coauthor is sincerely acknowledged:

Dahal, B., and Mishra, D. (2018). "Effect of geogrid inclusion on ballast breakage: A numerical study using the discrete element method". Proceedings of the 2019 Geosynthetics Conference, February 10-13, 2019, Houston, Texas.

Introduction

Type of aggregate (in terms of geology), particle angularity, gradation, and relative arrangement of individual particles in the aggregate matrix are the primary factors that influence the elastic as well as inelastic response of railroad ballast layers under loading (Tutumluer et al., 2007). Accumulation of irrecoverable strain or permanent deformation within the ballast layer is caused by rearrangement and breakage of individual ballast particles, and is the main trigger for maintenance activities on railroad tracks (Kwan, 2006). Geosynthetics have been proven in the past to reduce particle degradation and the resulting permanent deformation accumulation in ballast layers, thereby improving the overall track performance (Brown et al., 2007; Indraratna et al., 2006; Indraratna and Nimbalkar, 2013). Geogrids, a type of geosynthetics, can be placed within the ballast layer to improve its strength and modulus. Interaction between individual particles and geogrid apertures restricts excessive lateral movement of ballast particles under loading (Brown et al., 2006; Qian et al., 2013).

The degree of interlock between the geogrid and ballast aggregates is affected by various factors like the aggregate particle shape and size, types and properties of geogrids, loading conditions, and compaction effort during the installation of geogrids (Qian et al., 2015). Researchers have conducted laboratory and numerical studies to study this reinforcement mechanism due to biaxial geogrids having rectangular or square apertures (Indraratna et al., 2006; Brown et al., 2007) and triaxial geogrids having triangular apertures (Qian et al., 2013). Most of these past research efforts observed increased bearing capacity of the track substructure due to geogrid reinforcement. Biaxial geogrids have high tensile strength properties mainly in two directions, machine direction and cross-machine

direction, while triaxial geogrids can provide more uniform reinforcement in all directions (Qian et al., 2013); several research studies have compared the performances of these two geogrid types as far as reinforced ballast response under loading is concerned (Tutumluer et al., 2009; Biabani and Indraratna, 2015).

Studying the interaction between geogrid and ballast particles at a micromechanical level can enhance the understanding of reinforced ballast behavior under loading. Analysis at the micromechanical level is particularly important when comparing the degree of ballast degradation under unreinforced and geogrid-reinforced conditions. An ongoing research study at Boise State University is using the Discrete Element Method (DEM) to understand the effect of geogrid reinforcement on ballast breakage and the associated vertical permanent deformation of the ballast layer. Particle breakage and permanent deformation accumulation trends were studied for unreinforced ballast specimens along with biaxial and triaxial geogrid-reinforced specimens.

Modeling Approach

This research study marks an innovative use of the pavement design package (pdPkg) of Particle Flow Code in 3 dimensions (PFC3D). The pdPkg can be used for the creation and triaxial testing of synthetic unsaturated granular material with the geogrid embedment. Detailed explanation about the pdPkg can be found in the technical memorandum prepared by Potyondy (2018). Relevant model parameters for the models created in the current study have been borrowed from Potyondy (2018). The following sections briefly describe the procedure adopted to create the geogrid and ballast materials using the pdPkg.

Model Generation

Geogrid Reinforced Specimen

One of the primary considerations during numerical modeling involves selection of appropriate model dimensions. This is particularly important in case of discrete element modeling as the relative dimension of the model with respect to the maximum particle size can significantly affect the results. Indraratna et al. (1993) reported that as the value of sample size ratio (ratio of diameter of specimen to the maximum particle size dimension) approaches 6, sample size effects become negligible. Commonly used ballast materials often comprise particles as large as 50-60 mm; accordingly, to minimize size effects while at the same time keeping the computational time requirements within reasonable limits, a cubic specimen box of size 300 mm X 300 mm X 300 mm was selected for this study. Using the pdPkg, a geogrid set comprising one layer of flat geogrid oriented perpendicular to the specimen axis was then created, and placed at the center of the specimen box. Ballast grains represented by simple 4-ball clumps, satisfying the particle size distribution presented in Figure 4-1 were then distributed in the box. Note that the ballast shape selected in this study was an overly-simplified polyhedral shape and was selected to reduce computational efforts associated with more complex polyhedral particles. Movement of the grid was then fixed during this initial assembly stage such that no rotation or translation of the balls forming geogrid was allowed; and the ballast grains were distributed uniformly in the model until the static equilibrium was achieved. Confinement was applied by moving the specimen box walls to obtain a material pressure of 10 kPa. Note that this confining pressure level was selected as it has been reported in the literature as being representative of initial railroad ballast layer confinement pressure (Indraratna et al., 2010). After this

step, the grid was freed, and the above step was repeated on the unconstrained grid to allow the grid to move and deform in response to the compressive forces imposed by the grains. Detailed description of this grid embedment process in pdPkg can be found elsewhere (Potyondy, 2018).

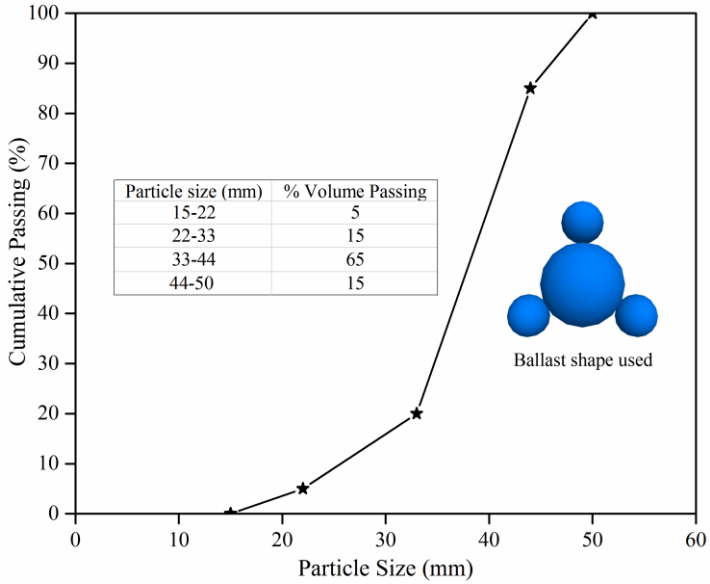

Figure 4-1: Particle size distribution used in the current study to create the ballast matrix (Inset: tetrahedral ballast clump used in the model)

Finally, at the end of this process, a specimen box consisting of homogeneous, isotropic and well-connected ballast assembly with an embedded and well interlocked grid at the material pressure of 10 kPa was produced. A total of 846 ballast clumps (each clump comprises four balls) were created. One of the primary objectives during the sample preparation phase was to generate ballast assemblies with similar porosity values. The final porosity values achieved for the three different geogrid-reinforced models (biaxial beamed, biaxial parallel bonded and triaxial beamed; details to be provided later), were 0.462, 0.460 and 0.460 respectively. Note that final porosity values in the range of 0.44-0.46 were

targeted as it has been reported by researchers to be the realistic porosity value of the railroad ballast layer (Indraratna et al., 1998).

Geogrid Properties

Two different types of geogrids, based on the aperture shape, were modeled in the current study: square (biaxial) and triangular (triaxial). Figure 4-2 shows the DEM-generated geogrid elements used in the current study. Note that each grid consists of strings of overlapping spherical balls joined in a particular manner. For biaxial geogrids, the bonds between individual particles were modeled using parallel bonds or beamed contacts; for triangular-aperture geogrids on the other hand, only beamed contact models were used between individual balls. These contact models provide the behavior of a finite size, linear elastic and bonded interface that carries a force and moment. The interface of the parallel-bonded contact model has a circular cross section, while the interface of the beam contact model has a rectangular cross section. Each grid behaves either as an elastic beam of circular cross section with varying radius along its length (parallel-bonded contacts), or as a prismatic and bisymmetrical elastic beam with varying width and height along its length (beamed contacts). The grid behaves as an elastic body which does not break, and will return to its original shape when unloaded. More details about the grid modeling approach can be found elsewhere (Potyondy, 2018).

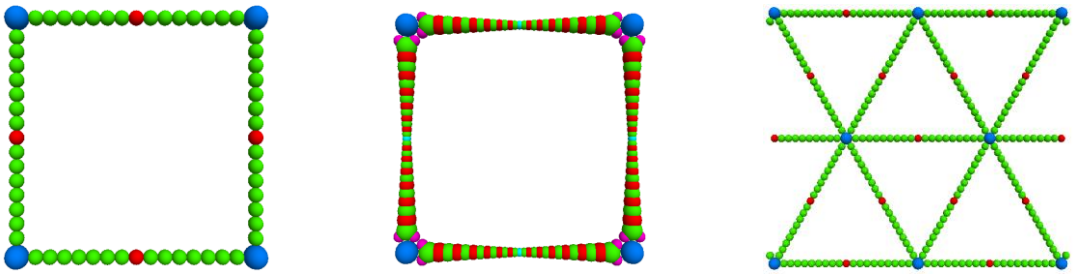

Biaxial Beamed (BB) Biaxial Parallel-Bonded (BP) Triaxial Beamed (TB)

Figure 4-2: Geogrid types used in the study

The properties of the square (BB/BP) and triangular geogrids (TB) resemble those of Tensar SS20 biaxial (aperture size 39 mm) and Tensar TX160 triaxial (pitch 40.7 mm) geogrids respectively. Detailed descriptions about the particular types of geogrids can be found elsewhere (Potyondy, 2018). Model parameters assigned within the Pavement Design Package to model the geogrids have been listed in Table 4-1.

Table 4-1: Model Parameters used to Define Geogrid Behavior

Grid Set parameter	PFC parameter	BB and TB Grid	BP Grid
Grid Density (kg/m^3)	gd_density	950	950
Young's Modulus (GPa)	gd_E	1.2	-
Poisson's Ratio	gd_nu	0.42	-
Grid Effective Modulus (GPa)	gd_emod	-	0.7
Grid Stiffness Ratio	gd_krat	-	2
Grid-Ballast Effective Modulus (GPa)	gd_ggemod	3	3
Grid-Ballast Stiffness Ratio	gd_ggkrat	2	2
Grid Ballast Friction Coefficient	gd_ggfric	0.5	0.5

Unreinforced (or Control) Specimen

Unreinforced (or control) specimens were created in the DEM model targeting the same specimen size as the geogrid-reinforced models; one of the objectives was to ensure the number of ballast particles are similar in the unreinforced as well as geogrid-reinforced specimens. However, upon 'material generation' in the model, it was observed that the porosity value for the unreinforced model was much lower compared to that for the geogrid-reinforced model. Significant differences in porosities can lead to significantly different particle interlock, thus resulting in noticeably different response under loading. For example, permanent deformation accumulation in a ballast layer depends mainly on the initial compacted density of the ballast (Selig and Waters, 1994). To facilitate direct comparison between unreinforced and geogrid-reinforced ballast behavior and to adequately isolate the effect of the geogrid reinforcement, it is critical that both specimens

be constituted at relatively similar porosity values. Therefore, the current study adopted the following approach to achieve the target porosity values.

First, a relatively larger (compared to that for the unreinforced specimen) box size (310 x 310 x 335 mm) was created, and filled with ballast particles. A total of 847 ballast particles (each particle comprised 4-balls glued together in a pre-established geometric pattern) were distributed in the specimen box using the same particle size distribution as shown in Figure 4-1. The side walls of the model were then compressed to achieve an average material pressure value of 10 kPa. The resulting change in dimension of the specimen produced a ballast assembly with a final porosity value of 0.464.

Contact Models Used

Five different types of contacts are possible in the models created in this current study. They are: (1) Ballast-Ballast; (2) Geogrid-Geogrid; (3) Geogrid-Ballast; (4) Ballast-Specimen Box; and (5) Geogrid-Specimen Box. Depending on the nature of interaction at these contact points, different contact models were assigned to mechanically define the behavior at these interfaces. For example, the beamed or parallel bonded contact models were used to define the behavior at the contact points between balls constituting the geogrids. Similarly, the Hill contact model (Potyondy, 2016) was used to define the behavior at ballast-ballast contact points. Finally, the linear contact model was used to define the grid-ballast, grid-specimen box, and ballast-specimen box interactions. The primary difference between the ‘beamed’ and ‘parallel bonded’ contact models was described earlier in this manuscript. Detailed information about the principles governing the linear contact model can be found elsewhere (Itasca, 2018).

The Hill contact model defines the behavior of an infinitesimal, nonlinear elastic (no tension) and frictional interface that carries a compressive surface interaction force and may carry a tensile moisture force. It behaves like two locally elastic spheres that may have a 'liquid bridge'. The liquid bridge is present if the moisture state is wet, and absent if the moisture state is dry. Detailed information on the Hill Contact Model can be found elsewhere (Potyondy, 2016). In the current study, the ballast material was modeled in a dry state, and therefore, the liquid bridge was not modeled. Therefore, each contact point between ballast particles simplifies to a non-linear elastic (no tension) contact with frictional interface.

Model Parameters Used

As already mentioned, one of the objectives of the current research effort was to study the effect of geogrid reinforcement on ballast breakage using DEM. To achieve this objective, it was necessary to first establish the crushing strengths for ballast particles being included in the model. This would help define the bond strengths between individual balls within each clump (remember that ballast particles were modeled as 4-ball clumps). This was accomplished by running the Single Particle Crushing Test (SPCT) in the laboratory. Once the particle crushing strengths were established in the laboratory, similar tests were performed using PFC. The Diametral Compression (DC) or Brazilian test, built into the material modeling package in PFC was used for this purpose. Figure 4-3-a and Figure 4-3-b show photographs of the SPCT being carried out in the laboratory. Figure 4-3-c and Figure 4-3-d show the same test being carried out in PFC. Note that special care was taken to replicate the exact ballast particle shape for DEM simulation of the SPCT. This was done using the software "Autodesk ReCap Photo" (Autodesk, 2017). Note that the red discs

in Figure 4-3-d represent broken bonds between individual balls. Appearance of the red disc indicates fracture of the ballast particle at that particular point. Three different ballast particles were tested in the laboratory using SPCT and were subsequently modeled using PFC. Bond strengths were assigned within each ballast clump after calibration of the Brazilian test models against the laboratory test results.

Table 4-2 shows the model parameters used in the simulation. Details about the ballast particle generation for SPCT and calibration of the SPCT model are beyond the scope of the current manuscript and will be published elsewhere. Laboratory specific gravity tests were conducted on the ballast particles, and the resulting values were assigned in the model.

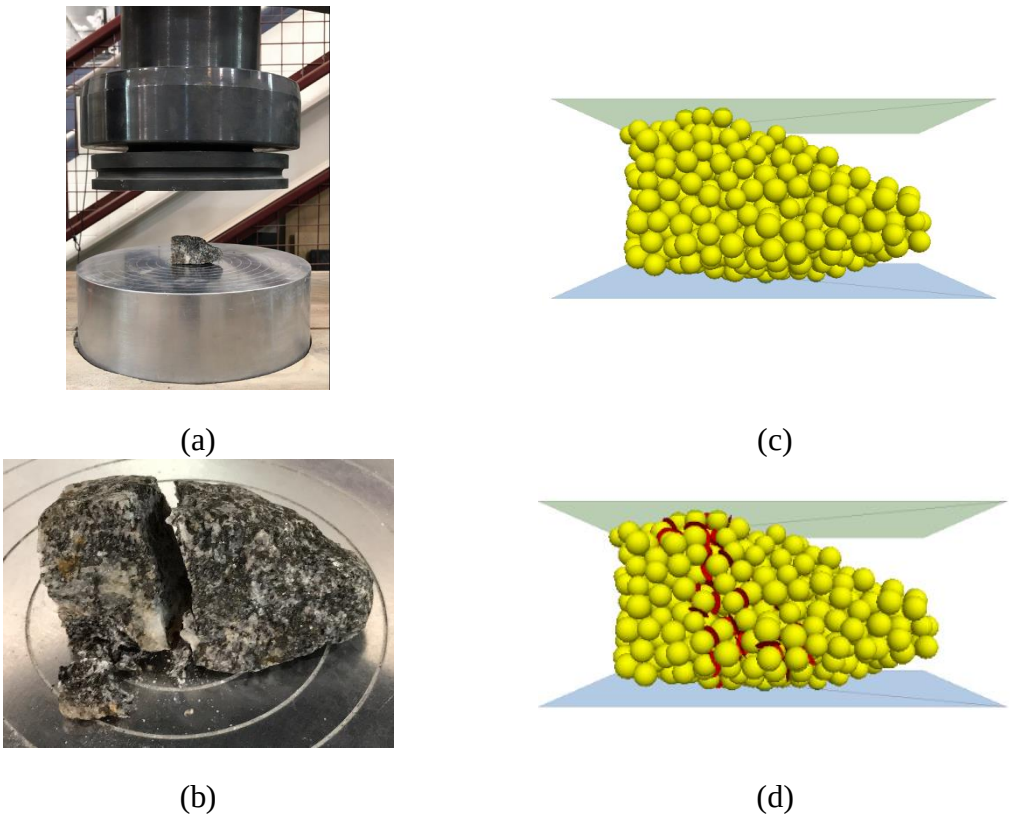

Figure 4-3: (a) Photograph of ballast particle on loading platen for single particle crushing test in the laboratory (b) Broken ballast particle after crushing (c) Ballast particle generated in PFC, and oriented for the Diametral Compression test (d) Fractured ballast particle after DC test (red discs represented fragments)

Table 4-2: Model Parameters used in the Simulation

Model Parameters	**Value**
Wall Effective Modulus	$3x10^9$ N/m^2
Ballast Young's Modulus	$8.33x10^8$ N/m^2
Ballast Poisson's ratio	0.2
Ballast Friction Coefficient	0.6
Ballast Density (ρ)	2610 kg/m^3
Parallel Bond Properties	
Parallel Bond Normal Stiffness ($\bar{k}_n$)	$1.48x10^{11}$ N/m^3
Parallel Bond Shear Stiffness ($\bar{k}_s$)	$7.58x10^{10}$ N/m^3
Parallel Bond Normal Strength (σ)	$3.83x10^6$ N/m^2
Parallel Bond Shear Strength (τ)	$1.57x10^7$ N/m^2
Parallel Bond Radius Multiplier (λ)	1

Figure 4-4 shows screenshots of the DEM-generated ballast specimens (at the end of the initial packed assembly process), under both unreinforced as well as geogrid-reinforced configurations. After this step, a cyclic loading was applied to the specimen (using a wall servo mechanism) in the vertical direction with a mean stress level of 232 kPa. Note that until the start of the cyclic loading process, the ballast particles (represented by 4 ball clumps) were modeled as non-breakable.

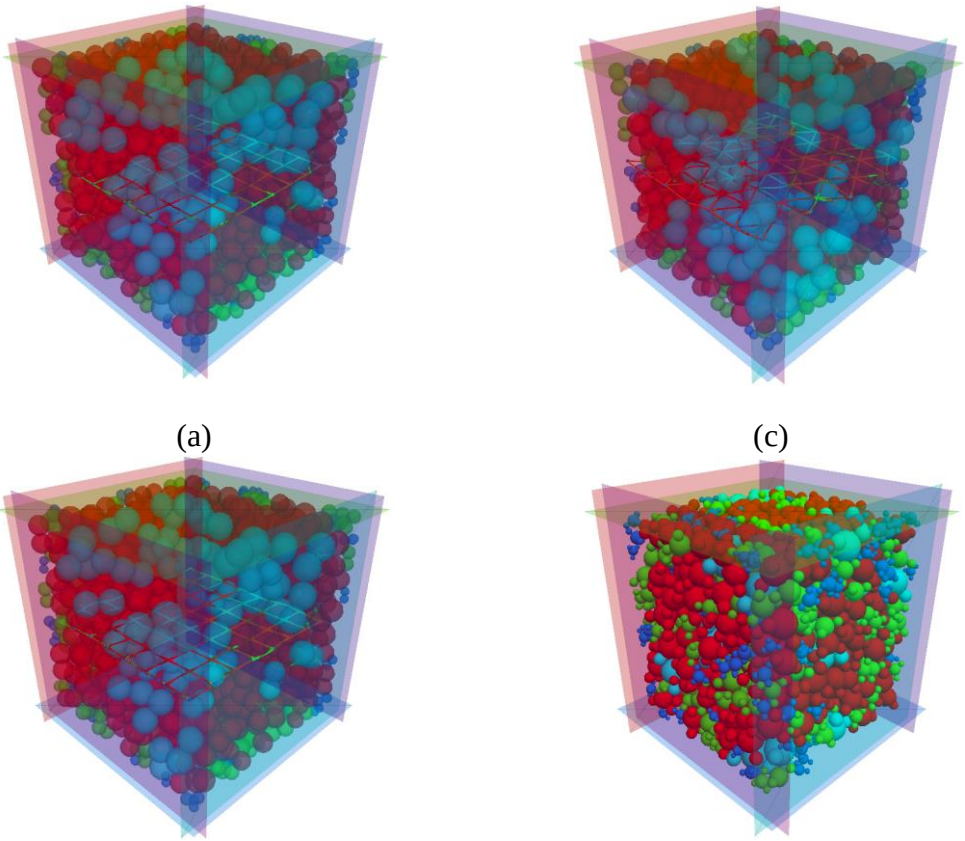

Figure 4-4: Initial packed assembly after ballast distribution and confinement (a) Biaxial Beamed or BB grid (c) Biaxial Parallel-Bonded or BP grid (c) Triaxial Beamed or TB grid (d) No-grid (The ballast particles have been made 50% transparent for a, b and c so that the embedded geogrid is clearly visible)

Ballast Breakage Simulation under Cyclic Loading

To allow the ballast particles to undergo breakage under cyclic loading, the ballast clumps were released, and parallel bonds with properties shown in Table 4-2 (section Parallel Bond Parameters) were applied in between the balls just before initiation of the cyclic loading process. At this state, each ballast particle behaves like a 4-ball cluster joined by the linear parallel bonds which could break when the stresses in the bonds exceeded the predefined bond strength values. Once a bond breaks, the resulting contact between ballast particles is governed by the Hill Contact model.

Sinusoidal load cycled between two compressive states of q_{min} (45 kPa) and q_{max} (419 kPa) was then applied via the top wall of the specimen box. The frequency of the cyclic loading was set to 10 Hz. Detailed description of the cyclic loading and the ballast breakage criteria can be found elsewhere (Dahal et al., 2018). As it would be unrealistic to perform simulations for a large number of cycles due to the limitation in computing times, the current simulations were run for 40 cycles; the number of ballast breakage as well as permanent axial strain accumulations for each model were recorded, and have been discussed below.

Results and Discussions

Comparing the Extent of Ballast Breakage

To quantify the number of bond breakages due to cyclic loading, the number of bonds before and after cyclic loading was counted. As seen from the table in the inset of Figure 4-5, the total number of bond breakages were very similar for the four different models, with the two extreme values differing by only 3% as far as the total number of bond breakages are concerned. Therefore, based on these results no clear distinction could be made regarding the effect of geogrid reinforcement on ballast breakage. This can be visually confirmed by plotting the particle size distributions for the specimens before and after loading. As seen from Figure 4-5, there was no significant difference in the particle size distribution after loading between the unreinforced and geogrid-reinforced specimens.

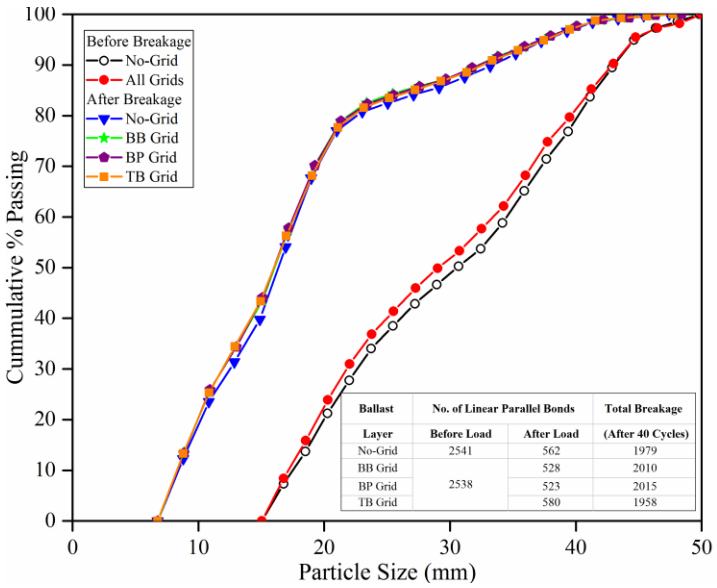

Ballast Layer	No. of Linear Parallel Bonds: Before Load	No. of Linear Parallel Bonds: After Load	Total Breakage (After 40 Cycles)
No-Grid	2541	562	1979
BB Grid	2538	528	2010
BP Grid		523	2015
TB Grid		580	1958

Figure 4-5: Ballast particle size distribution before and after cyclic loading (Inset: Table containing number of linear parallel bonds before and after cyclic loading for different models)

Comparison of Permanent Axial Strain or Permanent Deformation (PD)

Axial strain was calculated using the relative distance between the top and the bottom walls before and after cyclic loading. Figure 4-6 shows a plot of the permanent axial strain as a function of number of load cycles for different geogrid-reinforced and unreinforced specimens. As seen from the figure, for all the ballast layers, the permanent strain accumulation increased rapidly during the initial cycles of loading, and the rate of PD accumulation per cycle gradually reduced thereafter. The PD accumulation during the initial loading cycles is primarily due to ballast breakage and particle rearrangement. The unreinforced specimen showed the highest strain accumulation of approximately 15.4%. The grid-embedded ballast layers were found to accumulate total permanent strain magnitudes of 10.87% for BB grid, 10.71% for BP grid, and 9.99% for TB grid. From these results, the benefits of geogrid reinforcement for permanent strain reduction is clearly evident. Comparing the results for the biaxial and triaxial geogrids, the triangular-aperture

geogrids provided better aggregate interlock than the square aperture geogrids, and resulted in lower permanent strain accumulations. This can be attributed to the fact that the stiffness of triaxial geogrid is nearly consistent in all directions unlike the biaxial geogrids in which the stiffness is greatest in the direction of ribs only (Chen et al., 2012).

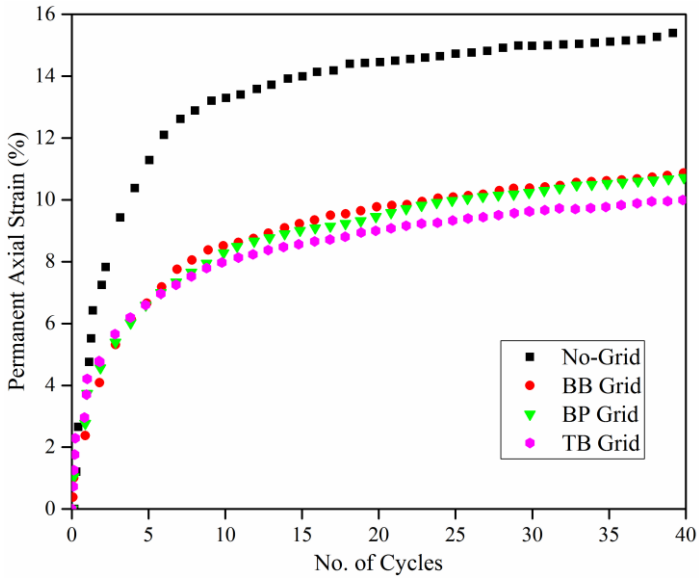

Figure 4-6: Permanent axial strain as a function of number of load cycles for different ballast layers

Conclusions

Based on the results of the above simulations, following conclusions can be drawn.

1. For both unreinforced as well as geogrid-reinforced ballast specimens, most of the permanent deformation accumulation and particle breakage occurred during the initial load cycles; this rate decreased as the number of loading cycles increased.
2. The use of geogrid in the ballast layer leads to significant reductions in the permanent deformation accumulation.
3. Triangular-aperture geogrids lead to greater reductions in permanent deformation accumulation compared to square-aperture geogrids.
4. No significant effect of geogrid reinforcement on ballast breakage was observed.

Limitations of Current Study

1. A simple polyhedral ballast shape was used in these models to reduce the computational effort requirements. Future publications will focus on models with more realistic ballast shapes.
2. The effect of geogrid reinforcement on lateral movement within the ballast layer was not studied; and will be included in future publications.

References

Autodesk Inc. (2017). Autodesk ReCap Photo, https://www.autodesk.com/products/recap/overview

Biabani, M.M., and Indraratna, B. (2015). "An evaluation of the interface behaviour of rail subballast stabilised with geogrids and geomembranes". Geotext. Geomembr. 43(3), 240-249.

Brown, S. F., Thom, N. H., and Kwan, J. (2006). "Optimising the geogrid reinforcement of rail track ballast". Railfound Conference, Birmingham.

Brown, S. F., Kwan, J., and Thom, N. H. (2007). "Identifying the key parameters that influence geogrid reinforcement of railway ballast". Geotextiles and Geomembranes, 25(6), 326–335.

Chen, C., McDowell, G.R., and Thom, N.H. (2012). "Discrete element modelling of cyclic loads of geogrid-reinforced ballast under confined and unconfined conditions". Geotextiles and Geomembranes 35, 76-86.

Dahal, B., Mahmud, S. N. M., and Mishra, D. (2018). "Simulating ballast breakage under repeated loading using the discrete element method". Proceedings of the 2018 Joint Rail Conference, April 18-21, 2018, Pittsburgh, PA.

Indraratna, B., Wijewardena, L. S. S., and Balasubramaniam, A. S. (1993). "Large-scale triaxial testing of greywacke rockfill". Geotechnique, London, U.K., 43(1), 37-51.

Indraratna, B., Ionescu, D., and Christie, D. (1998). “Shear behavior of railway ballast based on large-scale triaxial tests”. J. Geotech. Geoenviron. Eng., 124(5), 439–449.

Indraratna, B., Khabbaz, H., Salim, W., and Christie, D. (2006). “Geotechnical properties of ballast and the role of geosynthetics in rail track stabilization”. Ground Improvement, 10(3), 91–101.

Indraratna, B., Nimbalkar, S., Christie, D., Rujikiatkamjorn, and C., Vinod, J. S. (2010). “Field assessment of the performance of a ballasted rail track with and without geosynthetics”. J. Geotech. Geoenviron. Eng, 136(7), 907–917.

Indraratna, B., and Nimbalkar, S. (2013). “Stress-strain degradation response of railway ballast stabilized with geosynthetics”. J. Geotech. Geoenviron. Eng., 10.1061/(ASCE)GT.1943-5606.0000758, 684– 700.

Itasca. (2018). “Particle flow code in two and three dimensions”. Itasca Consulting Group, Version 5.0, Minneapolis, MN.

Kwan, C. C. J. (2006). “Geogrid reinforcement of railway ballast”. Ph. D. Thesis, University of Nottingham.

Potyondy, D. (2016). “Hill Contact Model [version 4]”. Itasca Consulting Group, Inc., Minneapolis, MN, Technical Memorandum ICG7795-L, October 12, 2016.

Potyondy D. (2018). “Pavement-Design Package for PFC3D [pdpkg13]”. Itasca Consulting Group, Inc., Minneapolis, MN, Technical Memorandum ICG16-8528-15TM, March 9, 2018.

Qian, Y., Tutumluer E., Mishra D., and Kazmee H. (2013). “Effect of Geogrid Reinforcement on Railroad Ballast Performance Evaluated through Triaxial Testing and Discrete Element Modeling”. Int. Society for Soil Mecs and Geotech. Eng.

Qian, Y., Mishra, D., Kazmee, H., and Tutumluer, E. (2015). “Geogrid-Aggregate interlocking mechanism investigates via Discrete Element Modeling”. Geosynthetics Conference

Selig, E. T., and Waters. J. M., (1994). “Track geotechnology and substructure management”. Thomas Telford Publications, London.

Tutumluer E., Huang H., Hashash Y., and Ghaboussi J., (2007). “Discrete element modeling of railroad ballast settlement”. AREMA 2007 Annual Conference

Tutumluer, E, Huang, H., and Bian, X. (2009). “Research on the Behavior of Geogrids in Stabilization Applications". Proc., Jubilee Symposium on Polymer Geogrid Reinforcement, September 8, 2009, London, UK.

CHAPTER 5: SUMMARY, CONCLUSIONS AND RECOMMENDATIONS FOR FUTURE RESEARCH

Summary

A commercially available three-dimensional Discrete Element Modeling (DEM) package, PFC3D® was used in this research effort to numerically study the importance of ballast breakage considerations on permanent deformation accumulation in railroad ballast layers under repeated loading. Initially, a breakable ballast layer model was created using simple ellipsoid ballast shapes, and cyclic train load was applied on this ballast layer to study the amount of breakage and permanent deformation under loading. Individual effects of parameters like no. of load cycles, vertical cyclic stress amplitude, loading frequency, particle size distribution and particle strengths represented by bond strengths were studied. After this step, three real ballasts particles were selected, and crushed in the laboratory to establish the individual crushing strength values. The lab-obtained test results were used to calibrate DE models of the particle crushing tests; the calibration process helped establish relevant model parameters that were used throughout the remainder of this research effort. Benefits of geogrid reinforcement of ballast layer was also studied by comparing the ballast breakage and permanent deformation trends for unreinforced and geogrid-reinforced ballast layers. Effect of geogrid types having different aperture shapes on ballast layer response under repeated loading was also studied.

Conclusions

Following conclusions were drawn based on the research reported in Chapter 2 of this thesis, and published as Manuscript Number 1: Dahal, B., Mahmud, S. N. M., and Mishra, D. (2018). "Simulating ballast breakage under repeated loading using the discrete element method". Proceedings of the 2018 Joint Rail Conference, April 18-21, 2018, Pittsburgh, PA.

1. Permanent Deformation (PD) accumulation under cyclic loading was very high for the model with breakable ballast particles compared to the one with non-breakable ballast particles. Most of the breakage as well as deformation occurred during the initial load cycles. As the number of load cycles increased, the percentage of ballast breakage as well as permanent deformation per cycle decreased, and became more stabilized towards the end of 50 load cycles.
2. With the increase in axle load amplitude, breakage as well as PD accumulation increased.
3. The effect of loading frequency was more pronounced for the ballast layer comprising non-breakable particles, compared to that comprising breakable particles. For the ballast layer comprising breakable particles, more breakage was observed for lower frequency values, but the total PD was comparable across different load frequencies after 200 load cycles.
4. With the increase in the bond strength values, there was less breakage and PD.
5. Increasing the ballast top size or removing the lower particle size from a given particle size distribution, both resulted in the decrease in PD.

Following conclusions were drawn based on the research reported in Chapter 3 of this thesis, and published as Manuscript Number 2: Dahal, B., and Mishra, D. (2019). "Simulating Polyhedral Ballasts Shapes to Study Ballast Layer Response under Train Loading". Journal of Computer and Geotechnics (in preparation).

1. It was confirmed that ballast breakage is the major factor that leads to the PD accumulation in the ballast layer.
2. Accurate representation of particle shape is critical while studying the response of ballast layers under repeated loading. On comparing the results for the ellipsoid and complex-shaped particles, having the same bond strengths, significant differences in the extent particle breakage and PD accumulation were observed.

Following conclusions were drawn based on the research reported in Chapter 4 of this thesis, and published as Manuscript Number 3: Dahal, B., and Mishra, D. (2018). "Effect of geogrid inclusion on ballast breakage: A numerical study using the discrete element method". Proceedings of the 2019 Geosynthetics Conference, February 10-13, 2019, Houston, Texas.

1. For both the geogrid-reinforced and unreinforced ballast specimens, the rate of ballast breakage as well as permanent deformation accumulation was very high during the first few load cycles. With the increase in the number of load cycles, both the rate of particle breakage and PD accumulation decreased, and stabilized towards the end of 40 load cycles.
2. Geogrid-reinforced ballast layers showed significant reductions in the PD accumulation.

3. Triangular-aperture geogrids performed better and led to greater reductions in PD accumulation compared to square-aperture geogrids.
4. No significant effect of geogrid reinforcement on particle breakage was observed.

Recommendations for Future Research

1. During the study of geogrid response under loading, simple polyhedral ballast shapes were used. As a further improvement to this research, real polyhedral ballast shapes can be simulated and also the effect of geogrid location in the ballast layer can be studied to know which geogrid location would be the best for extracting the optimum benefits from the geogrid-ballast interaction.
2. Effect of ballast breakage on tamping and the effect of tamped ballast layer under train loading can be studied to observe the benefits of tamping in terms of ballast breakage and PD accumulations.
3. Just recently in September 2018, PFC3D introduced the prerelease version of PFC 6.0 which is capable of simulating the polyhedral ballast geometry. The simulations carried out under the scope of the current master's thesis (approximating polyhedral and ellipsoid shapes by the agglomerates of bonded spheres); can be repeated using the real polyhedral ballast shapes to compare the results for actual polyhedral geometry simulation with the shape approximation used in the current study using agglomerates of bonded spheres.

References

Dahal, B., Mahmud, S. N. M., and Mishra, D. (2018). "Simulating ballast breakage under repeated loading using the discrete element method". Proceedings of the 2018 Joint Rail Conference, April 18-21, 2018, Pittsburgh, PA.

Dahal, B., and Mishra, D. (2018). “Effect of geogrid inclusion on ballast breakage: A numerical study using the discrete element method”. Proceedings of the 2019 Geosynthetics Conference, February 10-13, 2019, Houston, Texas.

Dahal, B., and Mishra, D. (2019). “Simulating Polyhedral Ballasts Shapes to Study Ballast Layer Response under Train Loading”. Journal of Computer and Geotechnics (in preparation).